Ernst-Abbe-Hochschule Jena
University of Applied Sciences

Master Thesis

Measurement of Hot Carrier Temperature using the concept of Johnson Noise Thermometry in the audio frequency bandwidth

Supervisor:
Prof. Dr. rer. nat. habil. Igor Konovalov
SciTec Faculty
Ernst-Abbe-Hocschule Jena

Author:
Niladri Bhattacharjee
Matrikel No. 643720

A thesis submitted in fulfilment of the requirements for the degree of Master of Science in Scientific Instrumentation

DECLARATION

I hereby declare that this Master Thesis entitled "Measurement of Hot Carrier Temperature using the concept of Johnson Noise Thermometry in the audio frequency bandwidth" was carried out by me for the completion of the degree: Master of Science in Scientific Instrumentation under the guidance of Prof. Dr. rer. nat. habil. Igor Konovalov, Ernst-Abbe-Hochschule, Jena, Deutschland. The interpretations put forth are based on my observation, understanding and experimentation work performed in the laboratory for the required objective and they are not published anywhere in the form of books, journals, social media posts, monographs and articles. Any contributions of others which are involved have been indicated, with due reference to the literature and acknowledgement of developments/discussions. I hereby certify that the above statements are true to the best of my knowledge.

Niladri Bhattacharjee

Place and Date

ACKNOWLEDGEMENT

This Master Thesis report, titled “Measurement of Hot Carrier Temperature using the concept of Johnson Noise Thermometry in the audio frequency bandwidth”, enlists my work performed for the completion of my MSc. in Scientific Instrumentation. The past year has been an exciting journey, dedicated to the last step in finishing my masters and I would like to express my sincere gratitude to those who helped me during this period.

I want to express regards to my supervisor Prof. Dr. rer. nat. habil. Igor Konovalov for giving me this opportunity to perform my master thesis in his team and be a part of his vision, while working at the EAH, Jena. I thank him for his patience, knowledge and guidance, provided throughout my time at the photovoltaic laboratory. His persistent guidance and unwavering enthusiasm kept me constantly engaged with my thesis work. His invaluable assistance and technical support helped me to structure, execute and improve this project.

I want to thank all the people, who have directly or indirectly helped, whether through their comments, feedback or suggestions throughout my journey.

Finally, I would like to express my gratitude to the people dearest to me. I am truly indebted of my parents, Mr. Debasish Bhattacharjee and Mrs. Sahana Bhattacharjee for their love, support and wisdom throughout my life. I also thank my family members, including my grandparents and my aunt, along with her family. Thank you for being part of this journey and for motivating me to pursue higher education in Germany, even when the distance was a hurdle. Last but not least, I express my thanks to my friends for their support and for boosting me during my thesis work. I have been encouraged, sustained, inspired and even tolerated by them. They indeed are my second family away from home.

ABSTRACT

Hot carrier solar cells, based on utilising the hot carriers' kinetic energy are designed with an absorber layer sandwiched between two electrodes. The hot carriers are extracted from the absorber layer before they thermalise. The temperature of these hot carriers is an important parameter in determining the parasitic energy flow between the hot carries and the phonon gas. Volumetric heat coefficient can be determined with the help of the temperature of these hot carriers thus, benefiting the search of new materials and structures as potential absorber layers. With this motivation, a methodology to measure the photoexcited hot carrier temperature is developed. The principle of Johnson Noise thermometry is extrapolated here for measuring this temperature. Hot carriers are treated analogously to thermal noise in semiconductors. A prototype of this methodology is built and characterised in the present study.

Advantages and flaws of the prototype are discussed further in this report. Samples of doped and undoped silicon, as well as graphite are tested upon. The probability of observing hot carriers in pure silicon chips is low and henceforth, this attempt did not result in acceptable results.

On the other hand, hot-carrier temperatures in the graphite samples were successfully measured through this approach though further research of graphite's behaviour is yet to be done. Thus, the attempts on silicon and graphite helped in determining the conditions to measure hot-carrier temperatures on other materials through this methodology.

Along with this, conclusive results upon the effects of the atmosphere making the sun's radiation noisy has been found and discussed. Finally, future modifications to improve the flaws in the prototype has been presented at the end of this study that paves the path for future development of the setup to measure the hot-carrier temperatures successfully.

CONTENTS

LIST OF FIGURES

LIST OF TABLES

1 INTRODUCTION

The development of highly efficient solar cells has become significantly important with the continual growth of demand in renewable energy. The traditional solar cells, based on a single p-n junction, could achieve a theoretical efficiency of 33.7% according to the "The Shockley-Queisser limit" [3]. However, higher efficiency solar cells have become a necessity and thus, much research is taking place in this field. The most efficient laboratory prototypes that are presently used for photovoltaics are based on thin-film multilayered structures, achieving an efficiency of 40%, still within the theoretical limit of 86% under full concentration [4]. Third-generation solar cells are an emerging field of study that intend to overcome the current efficiencies and performance limits. These include photovoltaics based on Dye-Sensitized [5], Perovskite [6], Quantum Dots [7] and Hot-Carrier Solar cells [8, 9, 10, 11].

A hybrid solar cell based on utilising the "hot carriers" to achieve high efficiency is the "Hot Carrier Solar Cells" (HCSC). The objective is to extract the electrical energy of the Hot carriers at the band edges before they thermalise. It has the potential to achieve efficiencies of 65% under 1 sun and 86% under full concentration [12]. Utilising the carrier lifetime thus becomes highly significant and challenging. HCSC requires optimised filtering, especially at the contacts to slow down the cooling of the hot carrier gas and therefore, eventually utilise these carriers [9, 10]. One such structure to model the filtering of the hot carriers has been discussed in [11]. The temperature of the hot electron gas (or e-gas referred to as here) is a key parameter in determining the efficiencies of this HCSC. The problem of the flow of energy between the electron and phonon gas is still under study [13]. The interactions between them are material-specific and thus, the search for materials and structures to slow down the cooling rate becomes important.

Based upon the model proposed by Würfel in [8] and the model described in [11], the architecture of HCSC is similar to the conventional solar cells with an absorber layer sandwiched between the electrodes. Various methodologies have been proposed, such as energy or optical selective contacts [10, 14] or plasmonics [15] to extract the photogenerated hot carriers in the absorber layer. All these methodologies rely on extracting the hot electrons and hot holes through a filter with a narrow bandwidth which is necessary to ensure that the cooling of the hot carriers is delayed i.e. to slow down the fall of temperature of the hot carriers to the lattice temperature and thus losing them to the cold carriers. Another important reason for the narrow bandwidth of the filter is to avoid the injection of cold carriers into the absorber from the electrodes or the lattice [16]. Due to the narrow bandwidth of energy, hot carriers take longer to relax into lower states and cause the increase in the separation of the quasi Fermi-energies for the electrons and holes, as described in [8, 16]. The hot carriers illustrate analogous thermal noise, which was discussed by Nyquist in [17]. Thus, the steady-state Nyquist theorem can be extended to the hot carrier regime, which is discussed later.

With this motivation, the present research thus aims to measure the temperature of the photogenerated hot carriers using noise measurements in potential absorber layer materials. The measured temperature of the e-gas generated provides an idea of its volumetric heat capacity of a photoresistor and eventually, provides the framework of barrier design to filter the hot e-gas. The idea of Johnson Noise Thermometry [18] is extrapolated here to measure the hot-carrier temperature in these materials. The diffusion noise or the hot carrier noise presumes a quasi-equilibrium Fermi-Dirac distribution [8]. But as discussed in [19], the non-thermal hot carriers still hold an analogous relation to Einstein's electrical mobility equation describing the diffusion coefficient. This idea makes the hot carrier noise analogous to thermal noise. Most of the research to study hot carrier dynamics, until now, have been made using artificial laser systems [1, 10, 13, 20, 21]. Monochromatic laser radiation is a poor replacement for the spectrally extended sunlight. Altogether, the measurement conditions are very different under an optical-laser system from the conditions in a solar cell.

"The photoexcited carriers thermalise electronically via carrier–carrier scattering, producing a hot carrier distribution with an elevated temperature compared to the lattice" [20]. The elevated temperature of the hot-carriers compensates the photoresponse of the semiconductor material, which forms the underlying principle behind measuring the hot carrier temperature. The carrier temperature is determined from the noise generated under natural sunlight in the audio frequency range, i.e. 200-20000 Hz. With this idea, samples of silicon and graphite are illuminated with the sun and the thermal noise is recorded, which is then-after transformed into voltage equivalent and corresponding temperature. Silicon is selected as it is the most widely available and used semiconductor. While graphite, being a widely used semimetal might have the potential to be considered as an absorber layer. Thus, a new methodology of finding the temperature of highly excited photocarriers is presented here based on the idea of Johnson Noise Thermometry. The detailed analysis of this methodology is discussed in the next chapters.

The setup of the experiments is discussed next in brief following which a detailed characterisation of the equipment is presented where three amplifiers are discussed along with two possible input options to the computer. The best setup is selected and the experiments are performed on samples of silicon and graphite. The results are discussed and the possibilities of modifications are presented at the end of this study.

As known, the probability of observing hot carriers in silicon is low [20, 22]. Thus, this attempt of measuring the temperature of the hot carriers in silicon samples, in the audio range did not result in acceptable success due to the internal properties of silicon as well as external hindrances. Whereas, graphite showed the presence of hot-carriers and the carrier temperatures recorded through this approach might be considered as hot-carrier temperatures unless further insights are investigated.

The results obtained yet show some flaws in the methodology, especially because of the unsuccessful attempts with silicon. The positive results with graphite helped to draw the conditions for successful measurement of hot-carriers through this approach. It thus paved the path for future attempts of the same methodology using other materials. The analysis of the hindrances and also the possible solutions of them are also discussed further. The constraints in observing hot carrier dynamics limit the use of bulk material as well as a good lattice cooling mechanism becomes a necessity.

2 THEORY

2.1 Hot Carriers

Photoexcitation in semiconductors creates electron-hole pairs when the energy of a photon is more than its bandgap (i.e. interband-absorption). These photogenerated carriers have kinetic energy more than that of the lattice. They embed themselves deep inside the conduction band. The excited electrons lose their energy and relax to band minimum or maximum (only for holes) by various mechanisms such as phonon scattering or carrier-carrier scattering. In the case of an intense photoexcitation, this relaxation process leads to the formation of "hot electrons" and subsequently phonons [1]. A similar phenomenon occurs for the holes. These hot carriers are at a quasi-equilibrium state with the rest of the lattice. From Figure 1, it is seen that when a photon with energy hν_l is incident on a semiconductor lattice with bandgap E_g, such that h$\nu_l > E_g$, photo-generated electrons and holes are created, as depicted by the electron in Figure 1 with energy ΔE proportional to the $(h\nu_l - E_g)$. This hot-electron loses its energy to the lattice and become a part of the cold electron gas, i.e. become a cold carrier. This phenomenon of thermalisation takes place in the order of 10 picoseconds and has been discussed in [11] or studied by a double-spectrometer in [1]. In Figure 1, '1' and '3' corresponds to the generation of optical phonons and 2 represents the collision with the cold electron gas at the band-edge.

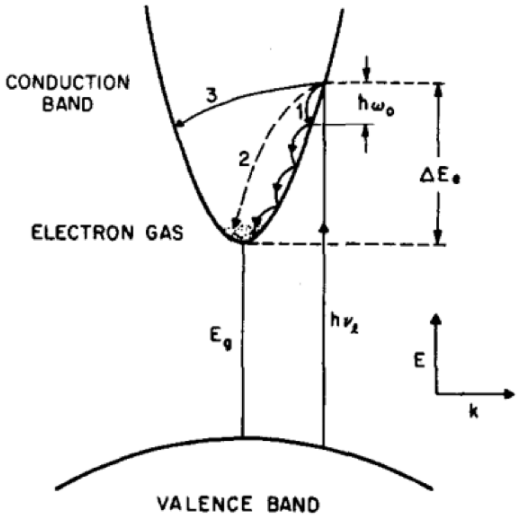

Figure 1: ***Schematic representation of various relaxation processes [1]***

The hot carriers have high kinetic energy which can be harnessed to increase the efficiency of the hot carrier devices. The absorption of the photons is governed by the bandgap E_g. Upon assuming ideal absorption situation, the maximum efficiency of 66% under 1 sun illumination is found for a bandgap of around 0.7 to 0.9 eV [16]. The absorption of the photons on semiconductors is governed by Beer-Lambert Law [23]. The absorption coefficient and the bandgap with respect to Figure 1 is related as: $\alpha(h\nu_l) \propto \sqrt{(h\nu_l - E_g)}$ for direct bandgaps. While for indirect bandgap, the absorption coefficient and the bandgap are related as: $\alpha(h\nu_l) \propto (h\nu_l - E_g \pm E_p)^2$ where E_p is the energy of the phonon that assists in the transition. A generalised Planck's Law for the hot carriers in semiconductors is presented in [24] while a detailed analysis of the absorption coefficient and hot carriers is presented in [25]. Hot carriers are dependent on the absorption spectrum from the sunlight, which is defined by the absorption coefficient.

2.2 Types of Noise in Semiconductors

Thermal Noise

Thermal noise or Johnson noise is created by the random motion of charges due to thermal excitation. The thermal motion of carriers creates a fluctuating voltage across the terminals of resistive elements. The RMS voltage is given by

$$v_{th}^2 = 4KTR\delta f$$

where v_{th} is the noise voltage generated through thermal excitation, K is the Boltzmann constant, T is the absolute temperature and δf is the bandwidth of measurement. From the power density, it is clear that the thermal noise is white noise. The spectral noise densities are constant up to frequency ranges of multiple THz and they are proportional to the resistance and temperature of the elements. It can be used in measuring the device temperatures as well as the quality of connections and contacts.

Shot Noise

Shot Noise is generated from random carrier arrival time across a barrier. It is seen as an unavoidable random statistical fluctuation of electric current when the carriers traverse the p-n junction. The RMS value of the shot noise current i_s is given by [26]:

$$\bar{i_s^2} = 2qI\delta f$$

where q is the electron charge, I is the forward junction current and δf is the measurement frequency. The power density is independent of frequency or temperature dependence. Thus shot noise is white noise. The measurement of the shot noise current is difficult as it is in the range of 10-100 μA. Shot noise current is used to characterise photodiodes, Zener diodes, avalanche diodes and Schottky diodes.

Generation-Recombination Noise

Generation and Recombination noise is seen due to the fluctuations in the number of charge carriers. Variations in the number of generation-trap-recombination centres lead to variance in resistance which is thus dependent on the temperature as well as biasing conditions. In the presence of several generation and recombination centres with varying lifetimes, the noise spectrum is the superposition of the different corresponding carrier lifetimes. The noise spectral density is a function of the carrier lifetimes as well as frequency.

1/f Noise

1/f noise or flicker noise or pink noise is a dominant noise in the low-frequency region and the spectral density function is proportional to 1/f. This noise is observed in all semiconductor devices under biasing. Examinations have shown the existence of this noise at extremely low frequencies up to 10 μHz. Different models have been predicted to analyse this noise as it becomes a limiting factor in the quality of semiconductor devices and more so in the nano-dimensions range. The origin of this noise is still under research but, the models developed by McWhorter in 1957 [27] and Hooge in 1969 [28] forms the basis of the study. Ideally, this noise originates from carriers being trapped and released by recombination centres with different lifetimes spread across the bulk of the semiconductor. For BJT transistors Hooge's model is more accurate in predicting the power density of the shot noise where he concludes the origin of the pink noise to be the scattering on silicon lattice. The 1/f noise can be described empirically in [29].

$1/f^2$ Noise

This is a derivative of 1/f noise. They are mostly observed at contacts, especially metallic contacts in integrated circuits. Connections with high current density experience this noise, especially due to electro-migration of the charges across the contacts. It gives a measure of the quality and reliability of contacts in the integrated circuits.

Burst or RTS Noise

This is another type of noise which affects when operating at low frequencies. This noise arises as pulses which can be visualised on the oscilloscope. With the given biasing condition, these pulses usually oscillate between two fixed voltage values but with varying duty cycles and pulse width. Biasing conditions and leakage from the power source may cause this type of noise. Though the spectral power density is similar to the generation-recombination noises as described above. The predominant cause of this noise is the occurrence of trap centres near the Fermi level. Contamination and lattice imperfection leads to the occurrence of such trap centres.

Burst noise is a function of temperature, mechanical stress, and also external radiation. In audio amplifiers, this type of noise is similar to the noise produced while making popcorn. They appear as random square wave pulses on the oscilloscope. Burst noise is significant in BJT amplifiers with a high β coefficient. Special BJT and FET have been developed with significantly low burst noise and thus are suitable for audio amplifiers.

Avalanche Noise

Avalanche noise is only seen in p-n junction devices which are operated in the reverse biased condition near the breakdown voltage. When a strong reverse biased is applied charges collide with each other with enough energy to knock-off new charges from the lattice. Avalanche noise, when occurs, is largest among any other type as described above. It is therefore sometimes, used as a noise source or a noise generator. The spectral density is independent of the frequency but proportional to the current.

2.3 .wav Format

Waveform Audio File Format is a popular audio file format used for storing audio bitstream in computers. It supports a variety of bit rates, multiple channels as well as bit resolutions. It takes into account the little-endian byte order of Intel CPUs [2]. It falls under Microsoft's RIFF specification of storing multimedia files [2]. The file format of .wav files is shown in Figure 2.

As seen in Figure 2, a wave file consists of a collection of various chunks for different properties and parameters of the file. The first 12 bytes, RIFF chunk descriptor, consists of the wave file headers and description of the format. The fmt subchunk enlists parameters describing the waveform, such as its sample rate. It occupies the next 24 bytes of data in the file. The next bytes, i.e. the data chunk consists of the actual data waveform. The .wav files can be visualised in the hex form, as seen in Figure 3. It shows the representation of bytes in a wave sound file.

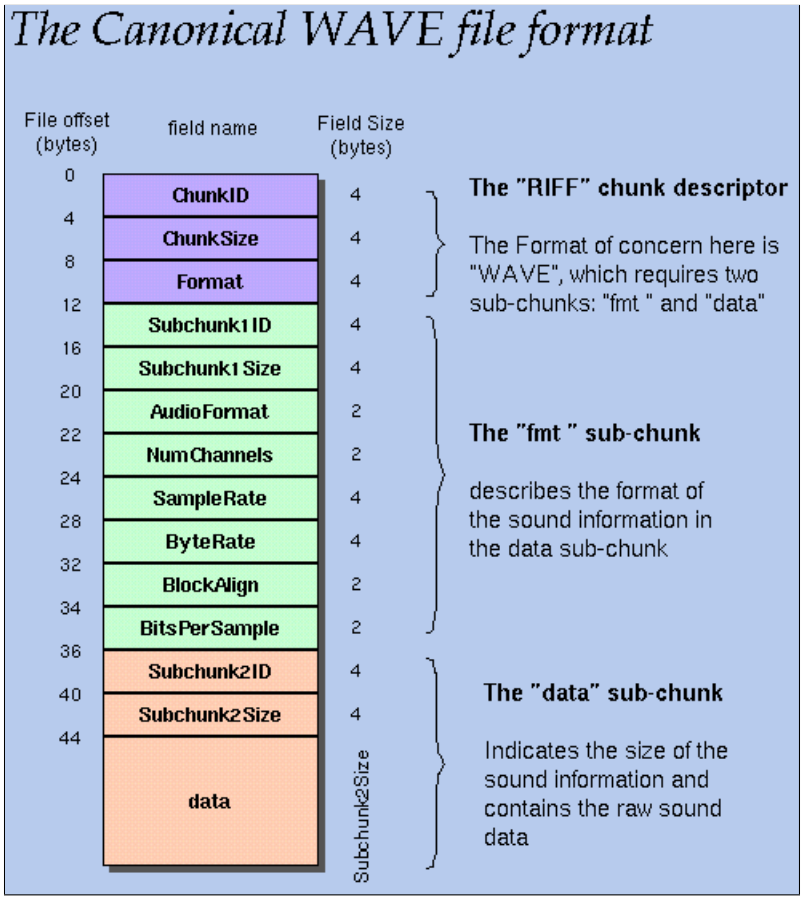

Figure 2: ***The Structure of Wave File Format[2]***

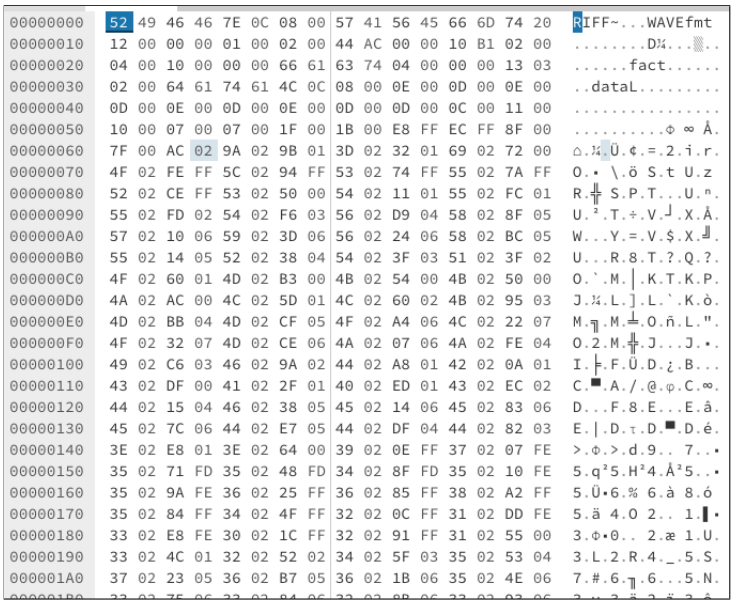

Figure 3: ***Hex representation of .wav on an editor***

2.4 Y factor for Noise Figure measurement

Amplifier noise can be categorised into external and internal noise. Internal noise may be due to [30]:

1. thermal agitation noise
2. shot noise
3. transit time noise
4. noise due to flicker, resistance effect and mixer generated noise

While external noise may include:

1. atmospheric noise
2. industrial noise
3. solar or cosmic noise

Noise figure represents the degradation of the signal and is given by [31]:

$$F = 1 + \frac{T_e}{T_o}$$

where T_e and T_o are the effective input noise temperature of the amplifier and the reference ambient temperature respectively. The Y-factor method, based on the Johnson-Nyquist thermal noise of resistors, is a widely used method for measuring the noise temperature of an amplifier. Upon plotting the output power of an amplifier against the temperatures of a resistor connected at the input, the amplifier noise temperature is obtained from the negative x-intercept of the curve. For a multistage amplifier, e.g. a two-stage amplifier with the first stage having a noise figure and gain F_1 and G_1 respectively and the second stage having a noise figure and gain F_2 and G_2; the net noise figure is given by:

$$F_{12} = F_1 + \frac{F_2 - 1}{G_1}$$

3 EXPERIMENTAL SETUP

In the present study to measure the temperature of the hot carriers generated in a semiconductor, a thin wafer is illuminated by the sun through a lens and the corresponding noise is analysed to find the temperature of the relatively "hotter carriers" compared to the rest of the lattice.

A noise signal is read from the semiconductor wafer by the computer and analysed to find a corresponding voltage equivalent to the temperature of the hot carriers. However, these weak noise signal generated needs to be amplified, for the computer to be able to record it. Thus the setup used is illustrated in Figure 4. The setup consists of a condenser lens, the semiconductor wafer on a sample holder (sample) to provide the necessary lattice cooling, audio amplifier and the computer where the noise signal is recorded and the voltage and the corresponding temperatures are calculated.

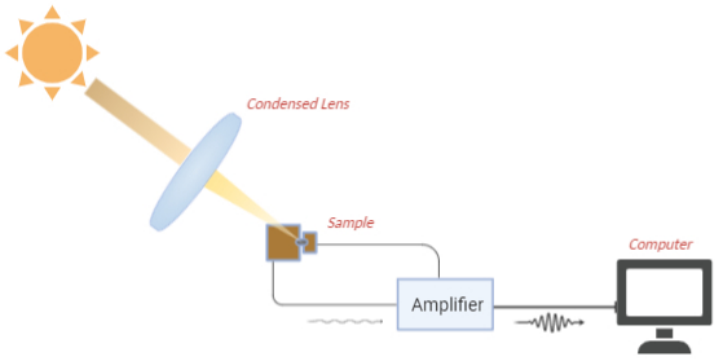

Figure 4: ***Primary Experimental Setup***

The semiconductor sample is illuminated through the condenser lens, which concentrates the sunlight to a bright 2 mm spot on the sample. The amplified noise signal is recorded by the computer in the form of a .wav file. A C++ program performs a high pass filtering on this recorded file and provides the user with a voltage corresponding to the highly excited carriers. From the idea described in [18], the deduction of the temperature of hot carriers is performed from the reference: the first ambient or the "dark" condition. In order to deduce the temperature of hot carriers from the samples, the following equation is used [18]:

$$T_{Hot-Carriers} = T_{ref} \frac{\overline{V_T^2}}{\overline{V_{ref}^2}} \frac{R_{ref}}{R_T} \tag{3.0}$$

where T_{ref}, $\overline{V_{ref}^2}$ and R_{ref} are respectively the temperature, average noise power of the first noise measurement made in dark and resistance of the sample in the dark. T_{ref} is the ambient temperature of 300 K. Whereas $T_{Hot-Carriers}$, $\overline{V_T^2}$ and R_T are respectively the required hot carrier temperature, average noise power of the sample and the resistance of the sample depending upon the conditions of measurement. When a dark measurement is performed, R_T is the resistance of the sample in the dark. While when a measurement of noise is performed under concentrated sunlight, R_T is the resistance of the sample under concentrated sunlight. Thus, when R_T and R_{ref} are nearly equal, the ratio is ignored. Further details and procedures are enlisted in Chapter 6 and Chapter 7.

Each of the modules shown in Figure 4 is discussed next. It is important to note that the differences between "hot-holes" and "hot-electrons" are not taken into consideration in the present study [32].

3.1 Sample

Samples of unintentionally doped or undoped silicon, p-type doped silicon and graphite samples are tested upon, through this method to measure the photoexcited hot carriers.

From the wafers of doped p-type Si and undoped Si, 2 mm x 2 mm chips are cut as illustrated in Figure 5. Two chips of undoped Si (A, B) and three chips of doped Si (A, B, C) are mounted on copper blocks as shown in Figure 6 which forms the samples for the present study.

The undoped silicon chips are cut from an intrinsic wafer by CrysTec. The wafer is S 5899 (1 0 0) with a resistivity of 3000 Ω-cm and a thickness of 300 μm. The doped silicon chips are cut from wafers of Sieger Consulting e.K., i.e. L14011 wafers (1 0 0) with a resistivity of 1-10 Ω-cm and thickness of 300 μm.

The silicon chips are contacted by burning in an aluminium paste at 940 °C (as shown in Figure 5) and is mounted on the copper blocks for lattice cooling using conductive epoxy which is cured at ambient conditions for 24 hours as shown in Figure 6. The samples are connected to the amplifier to detect the thermal noise. To record the drop in resistance under illumination in each of the samples, a Digital Multimeter (DMM) is used against the two copper blocks, as shown in Figure 25.

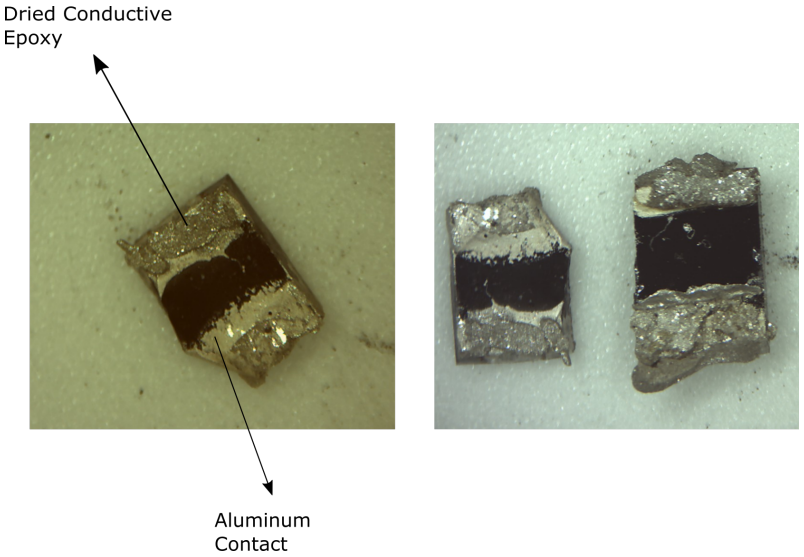

Figure 5: ***Aluminium Contacts on Silicon Wafers***

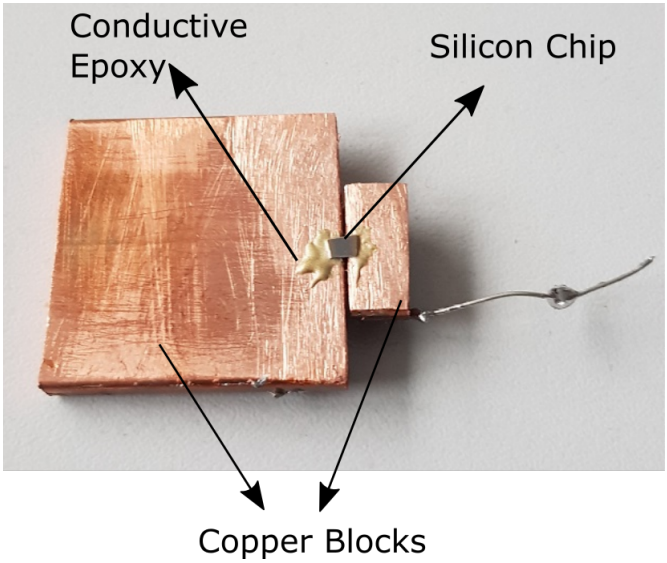

Figure 6: $2x2mm^2$ ***Silicon chip mounted on two copper blocks for contacting and cooling.***

Graphite samples are deposited on aluminium nitride (AlN) substrate by penciling with a graphite electrode from Polymet. Two samples are prepared for the measurements. Figure 7 shows the first sample, Sample A, directly prepared by Dr Konovalov, where graphite is deposited directly on the AlN substrate. Figure 8 shows the second sample, Sample B, which consists of Copper/graphite contacts. Between the two contacts, the same electrode is penciled again. This sample is prepared by Dr. Konovalov and Mr. Naidu. The sample template consisting of Copper/graphite contacts on AlN, prepared by Mr. Naidu, can be further used to test other materials, deposited between the two contacts. The AlN substrate is glued on a copper block with a thermal paste which provides a good heat dissipation path and keeps the lattice cool. The region between the two contacts is kept approximately 2 mm that is illuminated through the lens.

Figure 7: ***Sample A: Graphite penciled on AlN substrate, prepared by Dr. Konovalov***

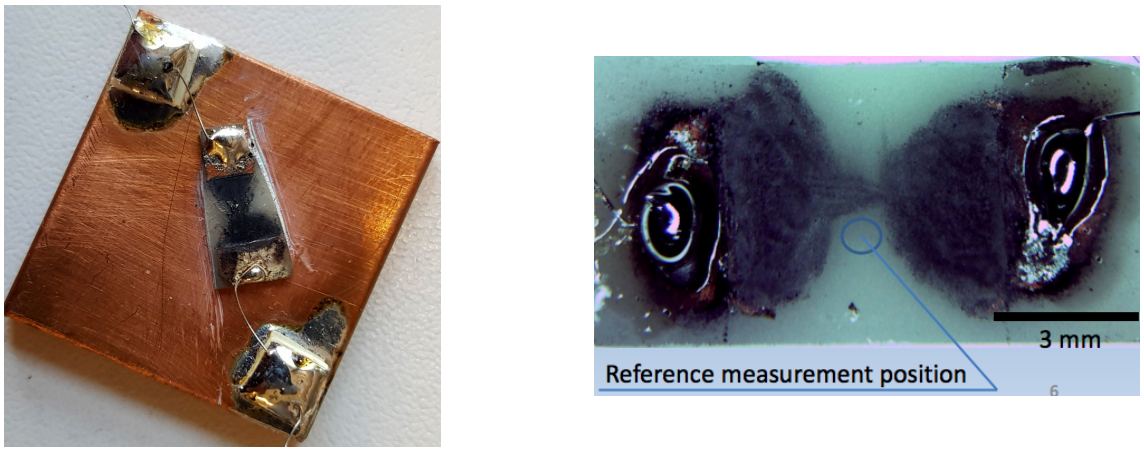

Figure 8: ***Sample B: Graphite penciled on AlN substrate, between Copper/Graphite Contacts prepared by Dr. Konovalov and Mr. Naidu***

3.2 Amplifier

The thermal noise generated in the semiconductor is a very weak signal for the computer to be able to detect with high sensitivity. Thus, the requirement of an amplifier is necessary. In the present study, low-frequency measurements of thermal noise are performed. Thermal noise being white, is independent of frequency dependence. For the low-frequency measurement, 200-20000 Hz is the range of the present experiments i.e. audio frequency range. Thus, a small signal audio amplifier is used.

The computer provides two inputs to record any audio input: the mic on the motherboard and the line input of the soundcard. Two amplifiers, shown in Figure 9 and Figure 10, are built and investigated further. The amplifier is shown in Figure 9 consists of a low-noise FET 2SK170 as a pre-amplifier, followed by two stages of general-purpose npn-BJTs 2N3904. Similarly, in Figure 10, the first stage consists of a npn-BJT BC550 that acts as a pre-amplifier, followed by two stages of 2N3904 biased in the same condition as in Figure 9.

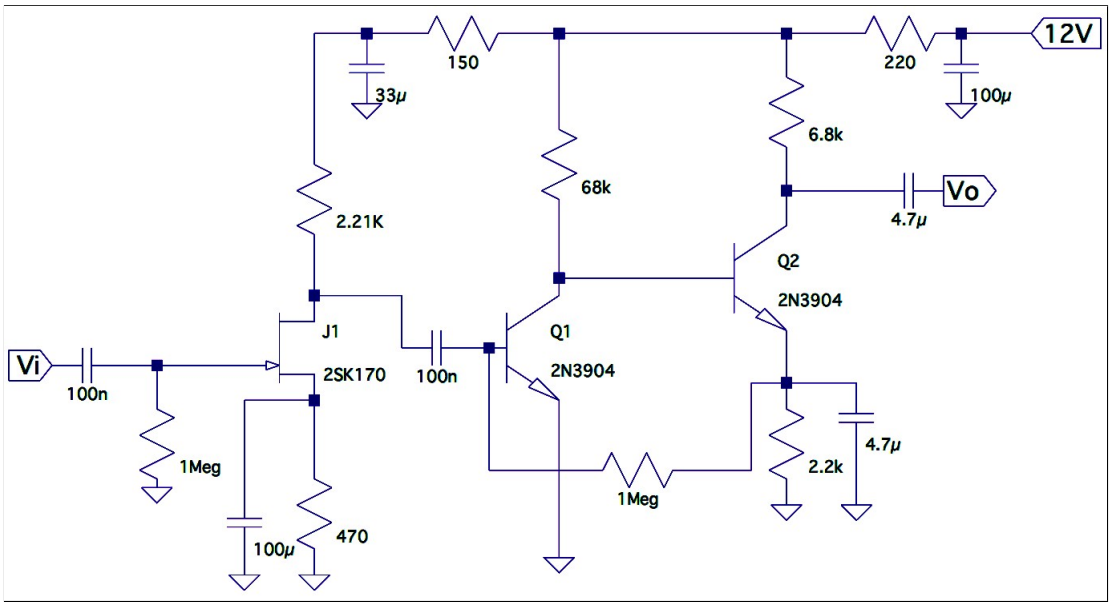

Figure 9: ***Amplifier 1: Audio amplifier with 2SK170 as the first stage***

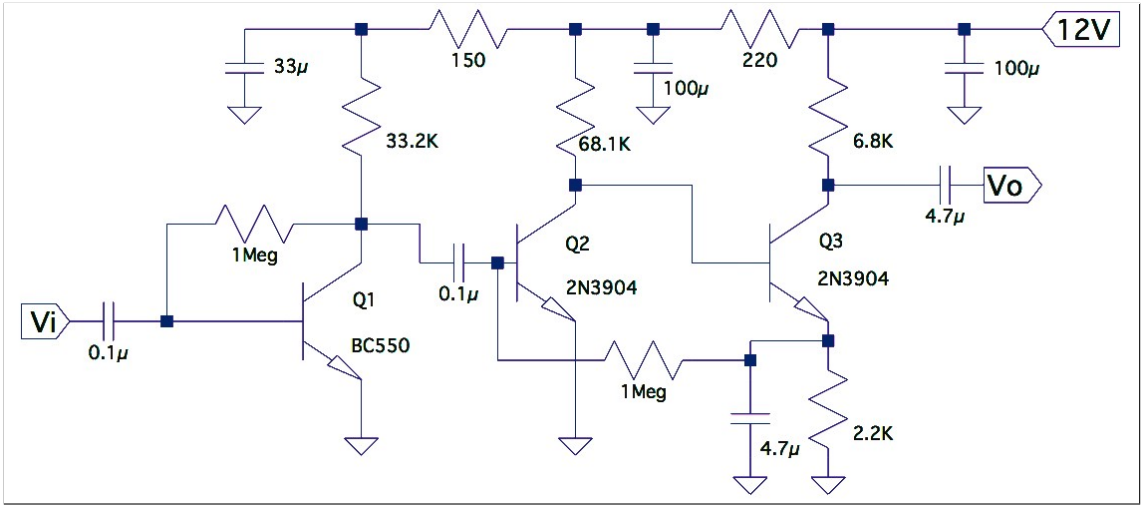

Figure 10: ***Amplifier 2: Audio amplifier with BC550 as the first stage***

The mic input provides high gain by itself. In contrast the line input provides better balance and lower gain. Thus, the amplifier shown in Figure 9 is modified to achieve lower gain as illustrated in Figure 11, which provides a better matching for the mic input.

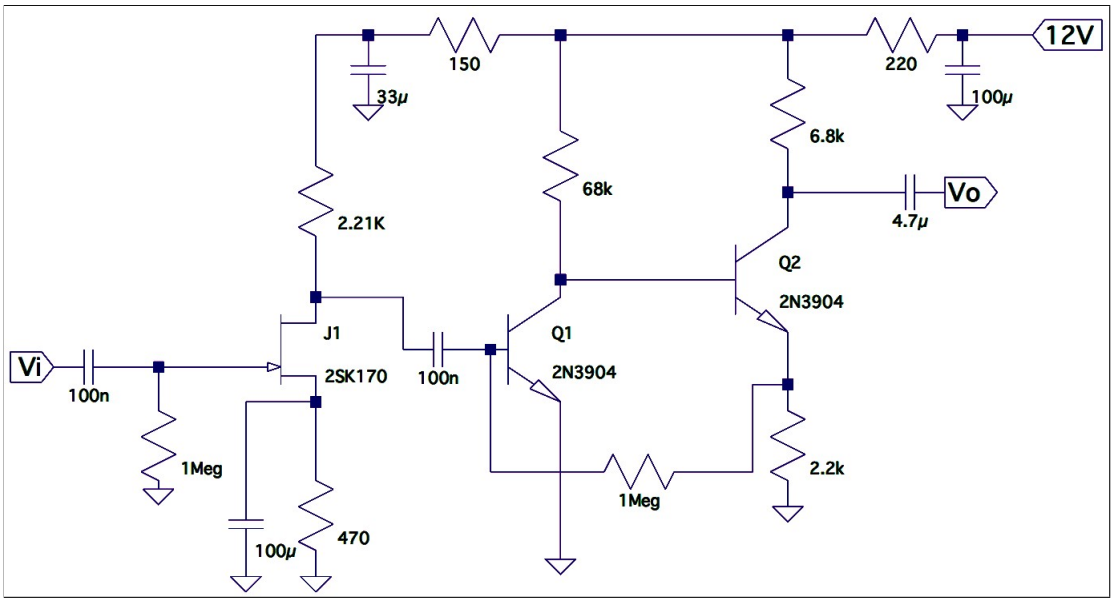

Figure 11: ***Amplifier 3: Audio amplifier with 2SK170 as the first stage with lower amplification than Amplifier 1***

Amplifiers in Figure 10 and Figure 11 are connected across the mic input of the motherboard while the amplifier shown in Figure 9 is connected across the line input of the soundcard. Further experiments and characterisation of the amplifiers, discussed in this section are performed and analysed in the next chapter. Note: For simplicity Figure 9, Figure 10 and Figure 11 are referred to as Amplifier 1, Amplifier 2 and Amplifier 3 respectively.

3.3 Software Tool

Following the recording of the file, a numerical representation of the recorded files becomes necessary. Thus, a C++ program is written and its flow is represented in Figure 13. This code opens the recorded ".wav" files as ".bin" files and reads the data in the form of hex. A high pass filtering is performed in the code. The result of this filtering provides a voltage equivalent in arbitrary units (a.u.) of the audio files.

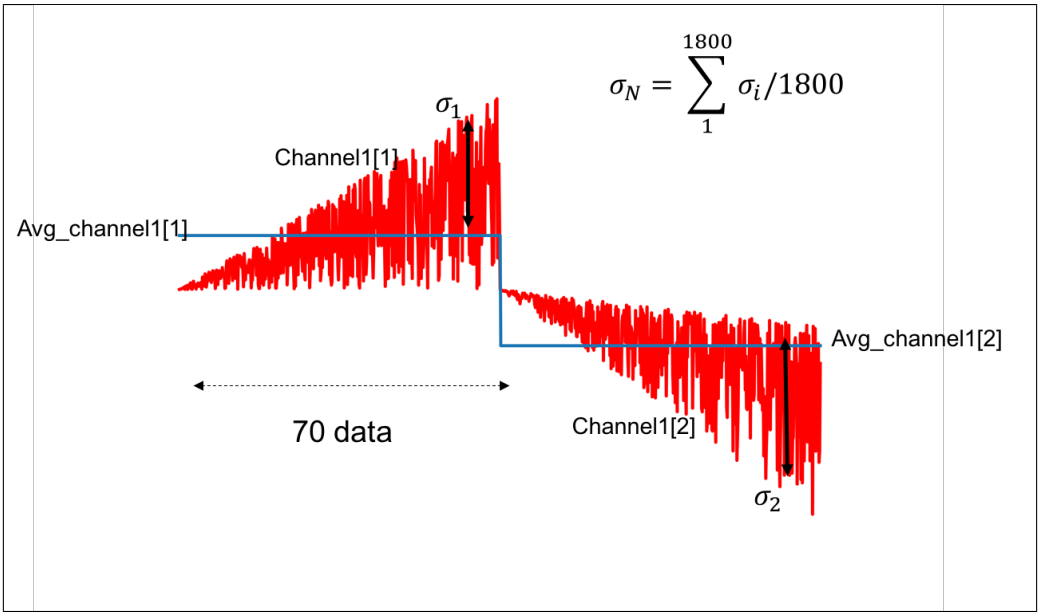

Figure 12: ***High Pass Filtering representation on data across Channel[1]***

Hot carriers in a semiconductor have higher energy and correspondingly higher temperature than the lattice or the cool carriers. To find the voltage of noise corresponding to the hot carriers, high pass filtering of the data is performed in the code. The illustration of the logic bridging between the hot carriers, recorded noise and corresponding voltage units is provided in Figure 12.

The code firstly skips over some data "chunk" which forms the header of the .wav file as seen in Chapter 2. The data is then read into channel1 and channel2, 70 data at a time, successively as described in Figure 13. The average and correspondingly standard deviation of these 70 data points are calculated and stored in new arrays. Again, the next set of 70 data points are read the process is repeated till the end of the file. Once this is finished, the average of the standard deviations (calculated and stored in the array before) is calculated and this is saved in the excel file which forms the equivalent voltage units of the hot carriers and thus the temperature of the hot carriers can be extrapolated. [Note that the voltage is still in arbitrary units.]

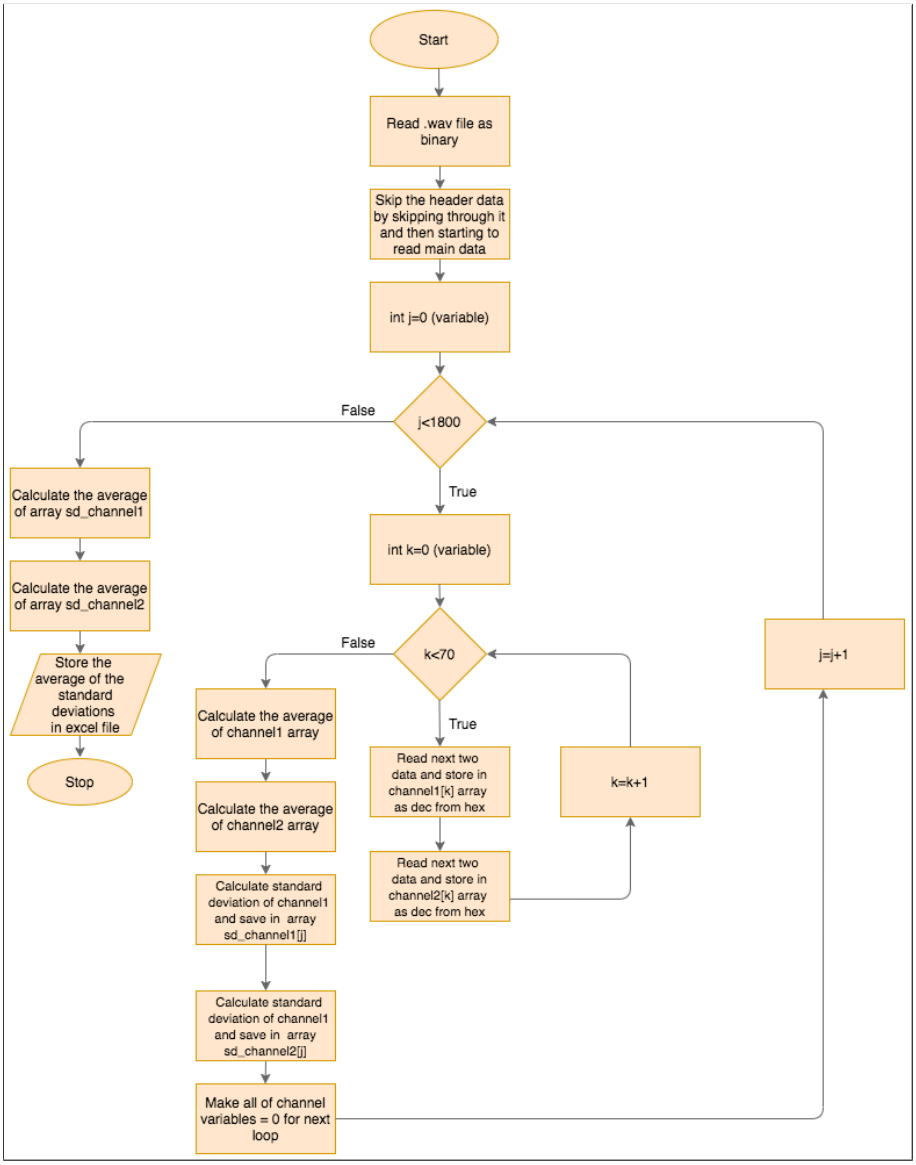

Figure 13: ***Flowchart of the C++ code***

3.4 Lens and Other Miscellaneous Requirements

- The lens used in the present study is a biconvex condensing lens of 5" diameter, which provides a bright 2 mm spot of the natural sunlight on the samples. The illumination side of the silicon chip is opposite that of the contacts, i.e. backside illumination. (Aberrations and imperfections of the lens are neglected in the present study and the sun's spot is assumed to be perfect.)
- The amplifiers are susceptible to external interference. Thus, a shielding box is built around it as shown in Figure 14. Though the interference is reduced, it is still non zer,o which is discussed later in this report.
- Two amplifiers of the one shown in Figure 9 are built to experiment with photodiodes to detect the effects of the atmosphere on the sun's radiation. The experimental setup and modifications are discussed in Chapter 9.

Figure 14: ***Amplifier with shielding box***

It becomes necessary to characterise the amplifiers before performing the main measurements. Thus, the next chapter is dedicated to finding the temperature of the equipment and also detect the internal noise of the equipment, i.e. determining the noise figure of the setup.

3.5 Experimental Procedure

The following steps are performed for all the samples to find the voltage equivalent and then the temperature from the recorded thermal noise:

1. The setup is connected, as shown in Figure 4. Recording of a noise file for 3 seconds, using the default audio recorder software is performed in the ambient condition without illuminating the sample through the lens. This becomes the first "dark" reading which is treated as the reference standard against which the other carrier temperatures are deduced from.
2. Once the dark reading is recorded, the sample is illuminated through the condensing lens. The change in noise under illumination is again recorded as a .wav file for 3 seconds. This file recording is termed as "Concentrated Sunlight"
3. Subsequently, a few more "dark" and "concentrated sunlight" recordings are performed for statistical results.
4. Once the recordings are performed, the C++ software discussed before compiles over all the recordings. Thus, voltage equivalents for the "dark" and "concentrated sunlight" are obtained in arbitrary units.
5. The voltage equivalents are squared to get a power equivalent of the thermal noise through the amplifier. The reference "dark" measurement owes to a room temperature of 300 K. Using eq. (3) the corresponding temperature in K is received, which is the resulting 'hot-carrier' temperature.

4 CHARACTERISATION OF AMPLIFIERS

In the present study of hot carriers' temperature, it is necessary to isolate the noise generated in the semiconductor chip from that of the equipment. Thus, in this chapter, the noise induced by the amplifiers as well as the corresponding experiments to study the properties of the amplifiers are discussed. Eventually, the best setup is selected among a comparison of three amplifiers and two inputs.

4.1 Noise Temperature and Noise Figure of the Amplifiers

In electronics, noise temperature is a fundamental and straightforward way to find the level of available noise power introduced by a component. Thus, to find the noise figure and the temperature, the Y-factor method is used. Suitable reference loads are attached at the input of the amplifiers. The loads are heated from one side and correspondingly the temperature of the loads is read using a thermocouple. At a various fixed temperature, the noise of the amplifiers is recorded for 3 seconds. This process is repeated several times for statistical results. The files are processed using the software tool, as discussed in Chapter 3.

Once the voltage equivalent of the thermal noise is found, the spectral power, as well as the corresponding noise temperature and the noise figures, are calculated. The noise temperature is calculated from the negative x-axis intercept of the plot for power vs. temperature. The noise figure is calculated from the formula

$$NF = 10 * log_{10}(1 + \frac{T_{sys}}{T_0})$$

where T_0 is the ambient temperature 300 K and T_{sys} is the noise temperature of the amplifier. Thus, the noise temperature and noise figures of each of the amplifiers discussed in Chapter 3 are calculated and analysed.

4.1.1 Amplifier 1

To study the noise temperature and noise figure of Amplifier 1, i.e. in Figure 9, connected across the line input of the soundcard, a 4.7 kΩ and a 47 kΩ load are attached at the input and heated till 423 K. The noise generated at specific temperatures are recorded for 3 seconds using the computer's default audio recorder application. The files are processed with the software tool explained in Chapter 3.

The recorded voltage power is plotted and the noise temperature is found from calculating the intercept of the curve with the X-axis.

Results

Figure 15 shows the plots of the arbitrary units of the voltage power corresponding to the thermal noise vs. the temperature, using the low-noise audio amplifier shown in Figure 9. The frequency range of measurement if from 200-20000 Hz. The temperature range of measurement is from 343-423 K. Figure 15a and 15b shows the plot of the noise power of the thermal noise which is obtained from the square of the arbitrary units of noise voltage for 4.7 kΩ and 47 kΩ respectively.

The extrapolation of the linear dependence of Figure 15a and of Figure 15b towards zero noise power results in a temperature intercept with the negative x-axis. This is the noise temperature. In Figure 15a, the noise temperature was found to be 240 ± 5 K while for the curve shown in Figure 15b, the noise temperature was found to be 36.5 ± 6 K.

The noise figure is found to be 2.11 dB for Figure 15a and 0.5 dB for Figure 15b. The possibilities of the differences in the noise temperature of the two curves have been discussed later in this chapter.

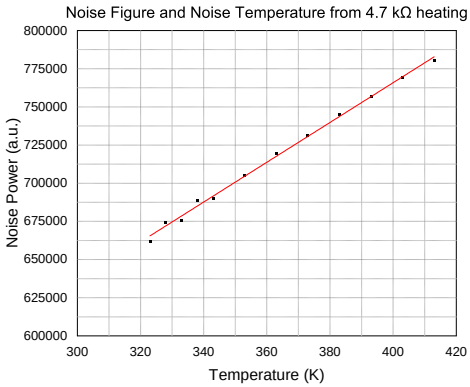

(a) ***Noise Figure and Noise Temperature from 4.7 kΩ***

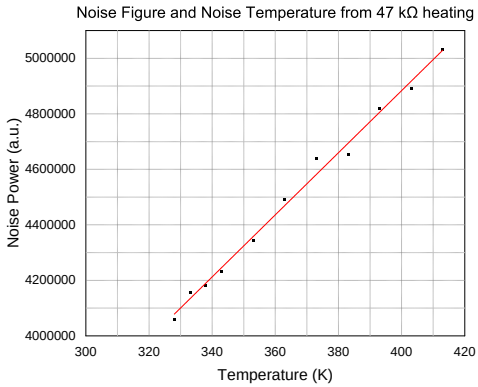

(b) ***Noise Figure and Noise Temperature from 47 kΩ***

Figure 15: ***Noise Power vs. Temperature for Amplifier 1***

4.1.2 Amplifier 2

The noise temperature and noise figure of Amplifier 2, i.e. in Figure 10, needs to be thus found. To do so again 8 kΩ and 22 kΩ resistors are put at the input of the amplifier and heated. The steps described above are repeated for this amplifier as well. It should be noted here that this amplifier is connected to the mic input of the motherboard.

The power of the noise signal against the temperature is plotted for both the resistances. The noise temperature and the noise figure are thus calculated as described above.

Results

Figure 16 shows the plot of the noise power vs. the temperature using the npn BJT BC550 as the first stage. Figure 16a provides the plot of the noise power obtained from the square of the noise voltage against temperature for 8 kΩ at the input. While Figure 16b provides the plot of the same for 22 kΩ. The frequency range of measurement is the same as before, i.e. 200-20000 Hz. Between the temperature range of 323-411 K, the measurements are taken.

Figure 16 shows the plot for two trials using 8 kΩ resistor and 22 kΩ resistors. For the 8 kΩ the noise temperature is found to be 3223 K and for the 22 kΩ the noise temperature was found to be 3152 K which are unrealistic. The corresponding noise figures were 10.69 dB and 10.6 dB, which provides the conclusion that this amplifier has a very high noise floor and thus, is not suitable for the study. It also provides an insight into the fact that the mic input may be noisier than the line input and provides automatic gain control (AGC).

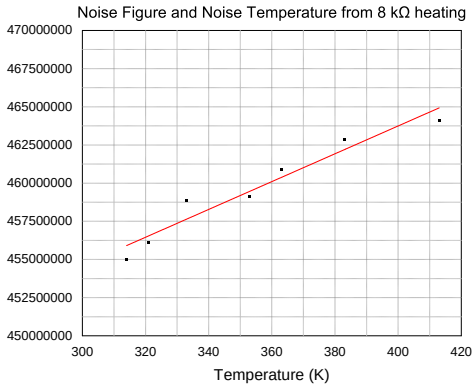

(a) ***Noise Figure and Noise Temperature from 8 kΩ***

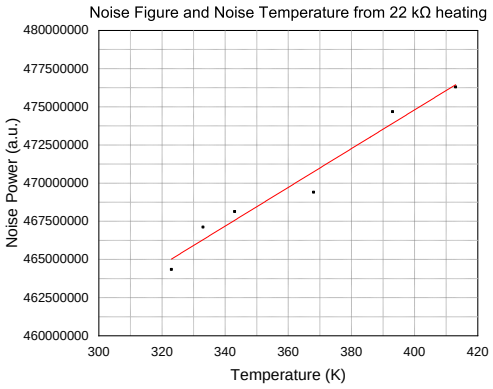

(b) ***Noise Figure and Noise Temperature from 22 kΩ***

Figure 16: ***Noise Power vs. Temperature for Amplifier 2***

To draw further conclusions into this argument about the mic input, Amplifier 1 is modified for lower gain as discussed in Chapter 3.

4.1.3 Amplifier 3

From the results of the noise figure of Amplifier 2, it becomes necessary to characterise the mic input further. For finding the noise temperature and the noise figure of the amplifier, the above-mentioned steps are performed again for Amplifier 3, i.e. shown in Figure 11. 8 kΩ and 22 kΩ resistors are connected to the input of the amplifier and steps mentioned above are repeated.

Results

The frequency range of the measurement is the same as before, i.e. 200-20000 Hz as well as the temperature measurement range of 320-425 K. The power corresponding to the thermal noise against the temperature is plotted in Figure 17.

From Figure 17, by repeating the steps before, the noise temperature is found by extrapolating the linear curve to zero noise power.

For the 8 kΩ the noise temperature is found to be approximately 170 K ± 10 K while for the 22 KΩ the noise temperature is 107 K ± 5 K. The corresponding noise figures for 8 kΩ and 22 kΩ are 1.95 dB and 1.32 dB respectively.

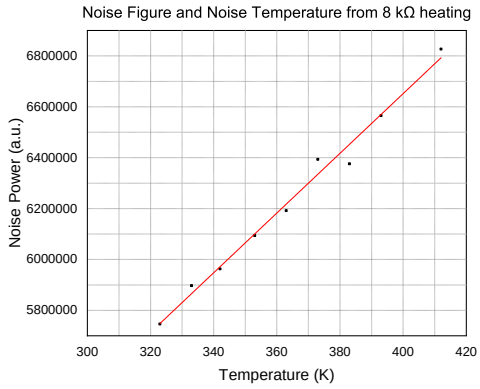

(a) ***Noise Figure and Noise Temperature from 8 kΩ***

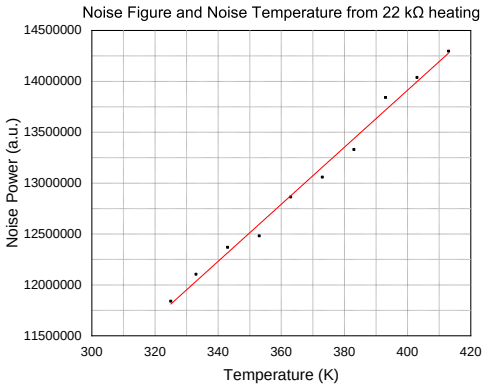

(b) ***Noise Figure and Noise Temperature from 22 kΩ***

Figure 17: ***Noise Power vs. Temperature for Amplifier 3***

Thus from these results, it can be analysed that the amplifier shown in Figure 10 has the highest internal noise while Amplifier 1 from Figure 9 has the lowest. Between Amplifier 1 and Amplifier 3, the higher noise figure of Amplifier 3 may be due to the mic input rather than the amplifier itself. Amplifier 2 and Amplifier 3 are connected across the mic input of the soundcard, which provides the feature of automatic gain control(AGC) and thus, manipulation of data is unavoidable unless it is manually turned off.

The mic input is a noisier, as well as provides higher gain, than the line input. The necessity to shift from mic input to line is an important criterion which needs to be analysed further.

It is essential to point towards the difference between the amplifiers here. In the amplifier shown in Figure 9, the first stage is a low-noise FET 2SK170 while the amplifier shown in Figure 10 uses low noise BJT BC550 at the first stage which is noisier than 2SK170 as specified in the datasheets. The first stage's noise figure dominates the noise figure of a multi-stage amplifier and therefore the differences between these two are necessary. Further details can be found in datasheets of the respective amplifiers.

It is also necessary to understand how the amplifiers react to different loads as it has been seen that the noise figure varies according to the load across the input. Thus, specifying tolerances in calculations of noise temperatures and figures is not discussed in detail because of its variation with the input resistor's thermal noise.

4.2 Different Loads across the Input of Amplifiers

Across the input of the amplifiers discussed so far, different load resistances are put, the noise of the equipment is recorded and processed using the software tool. The objective is to study the behaviour of the amplifiers with increasing thermal noise of the resistances at the input. It thus provides insight into load matching with the input impedance of the amplifiers. For noise signals to be optimally recorded, the load across the input terminals of the amplifiers must match with its input impedance.

Figure 18 shows the setup for testing different loads across the amplifiers. In the module of load, resistances ranging from 10 Ω to 1 MΩ are tested along with the short-circuit and open-circuit conditions.

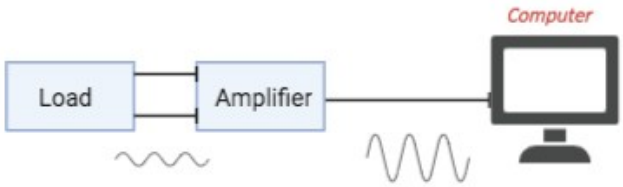

Figure 18: ***Block Diagram for the Load Matching Experiment***

Results

For each of the amplifiers, different resistances are tested. For Amplifier 2, shown in Figure 10, Figure 19 shows the plot of the noise voltage generated vs. the different resistances plotted on a logarithm (base 10) scale. In Figure 19, "theoretical noise voltage" is the thermal noise or the Nyquist Noise of a resistor, i.e. $v_{th} = \sqrt{4KTR\delta f}$. It shows the behaviour of the amplifier with varying resistances at the input, matched with the input impedance of the amplifier BC550.

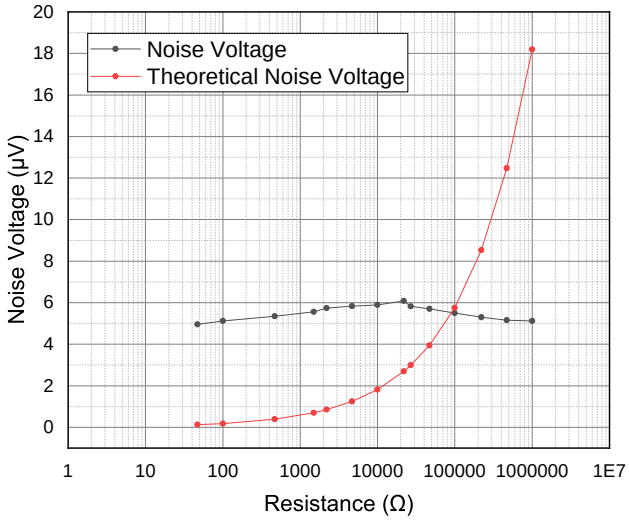

Figure 19: ***Plot of Noise Voltage vs. Different Resistances for Amplifier 2***

Figure 20 shows the response of the Amplifier 1, shown in Figure 9 against different resistances. The behaviour of the amplifier is again predominantly determined by the matching of the resistances with the input impedance of the FET 2SK170 amplifier. Again the 'theoretical noise voltage' in Figure 20 is the Nyquist noise of the resistors.

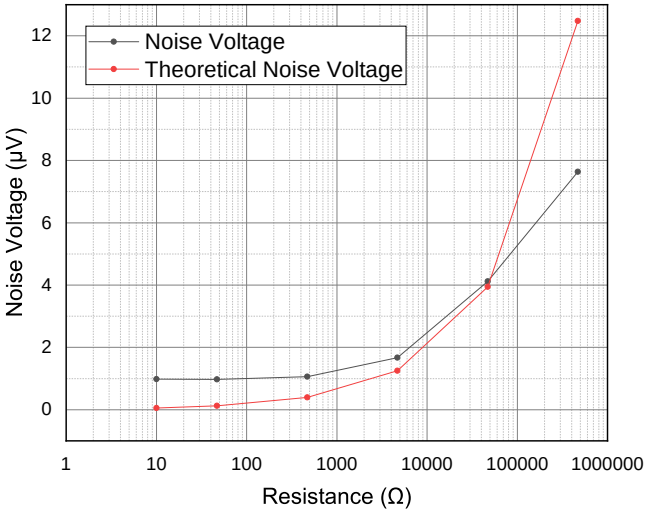

Figure 20: ***Plot of Noise Voltage vs. Different Resistances for Amplifier 1***

It is essential to understand the behaviour of both amplifiers. Amplifier 2 reads the thermal noise generated in the matched resistor at the input terminals. By connecting a load of 2 kΩ at the output and a signal generator at the input terminal, the input impedance of the amplifier is found to be 45 kΩ. From the plot in Figure 19 it is clear that closer the resistance across the input terminals is to the input impedance of the amplifier, higher is its sensitivity. But unfortunately, the thermal noise read by the amplifier does not replicate the theoretical noise after the order of 10 kΩ as seen in Figure 19. The signal generator provides a 195 mV signal at 20 KHz for the circuit. It is also evident that below 10 kΩ the noise recorded is higher than the theoretical noise. The equipment's internal noise contributes to this.

In Amplifier 1, the input impedance is found similarly to be approximately 1 MΩ with the signal generator providing 217 mV at 20 KHz of sinusoidal signal. As seen in Figure 20, the thermal noise of the resistor read by the amplifier matches the behaviour of the theoretical thermal noise of a resistor till the order of 100 kΩ beyond which the noise voltage detected by the amplifier is smaller than the theoretical noise of the resistor. Similar to Figure 19, here as well, the noise recorded by the amplifier is a little larger than the theoretical thermal noise, which is contributed by the amplifier's internal noise. It is also visible that the amplifier's internal noise depends upon the resistor at the input terminals, which is further discussed in this chapter.

It is clear from Figure 19 and Figure 20 that for smaller loads till orders of 10 kΩ both the amplifiers record the thermal noise correctly along with the equipment noise. For higher loads till 100 kΩ, Amplifier 1 is better suited. Beyond 500 kΩ the resistance across the input is close to the input impedance of the amplifier. Thus the amplifier sees two resistors connected parallel across the input terminals which are approximately close enough. Thus, a corresponding fall in the thermal noise is recorded by the amplifier. Thus the biasing is affected. Hence as a conclusion, amplifiers shown in Figure 9 and Figure 11 are better suited to read the input thermal noise across resistors at the input when the input resistors are between 100-10000 Ωorder.

The amplifier must be able to read the change in the thermal resistance across the samples by providing optimal gain, low noise and high sensitivity. These results are important as the amplifiers will see the change in resistance of samples under illumination as discussed in Chapters 6 and 7. *[Note: It is important to note that the voltage plotted is not in arbitrary units but in µV. The conversion factor between them is discussed later in Appendix 1]*

4.3 Gain of Amplifiers

To determine the AC voltage gain of each of the amplifiers, an input signal of 150 mV at 2 KHz is provided at the input of each of the amplifiers. Correspondingly, open circuit voltage at the output is noted and the gains are tabulated in Table 1.

Table 1: ***AC Voltage Gain of Amplifiers***

Amplifier	Vin (mV)	Vout (V)	Av	Av (dB)
Amplifier 1	150	3.442	22.94	27.2
Amplifier 2	150	4.512	30.08	29.56
Amplifier 3	150	3.228	21.52	26.65

The objective is to determine the AC voltage gain of the amplifiers as the voltage read and amplified by the amplifier should not overload the input to the computer, whether it's the mic input of the motherboard or the line input of the soundcard. To distinguish between the two inputs the following experiment is performed.

4.4 Line Input vs. Mic Input

Once the amplifier is selected, it becomes necessary to select which input suits the objective the best. As discussed before, there are two possible options available to record sound into the computer: the mic input of the motherboard and line input of the soundcard. The factors distinguishing the two inputs are the gain and the cross-talk between two channels during stereo recording.

Firstly, it is needed to look into the gain of the two inputs. By default, the audio recorder of the computer uses the motherboard's mic input to record. Automatic Gain Control(AGC) is a feature of Microsoft Windows which by itself is very good for regular recordings but a problem for the present study. What it does is, automatically adjusts the volume of the signal being recorded. That correspondingly means that the data being read gets altered and thereby, the data intended to be read in its raw form is manipulated. Thus, the actual results are not achieved concerning the present study. Therefore, to eliminate this problem, it can be turned off. However, the problem of high gain, higher noise and cross-talk between channels is still persistent. Line input of the soundcard provides better noise reduction and excellent isolation from leakage of data between channels. Figures 21a and 21b show the difference between the channels recorded through the line and mic input for a fixed input signal. With the same amplifier connected across the mic input and line input, a 22 kΩ is attached to the input terminals of the amplifier and heated. The experiment of finding the noise figure is repeated. Figure 21b and Figure 21a shows the two channels of a stereo recording. In Figure 21b, the computer saves the data of either of the channel into the other. Here the input is across channel 1 while the computer copied the data of channel 1 into channel 2. In Figure 21a, the cross-talk between the channels is still less. Again, the input of signal is across channel 1 while channel 2 is not connected. Thus as seen in Figure 21a, it is concluded that line input is chosen when cross-talk is needed to be avoided.

The problem of AGC altering the data is visible from the noise figure seen in Chapter 4 when the Amplifier 2 showed unrealistic noise figure. From the gain seen for Amplifier 2 as well as the noise figure across the mic input, it is clear that some of the data is either clipped or altered and this causes the noise figure and noise temperature to be so high. Though AGC can be switched off but the effect of cross-talk between two channels cannot be avoided for the mic input.

Thus, even though the line input provides lesser gain, it is better from the perspective of recording signals. The line input is thus chosen along with Amplifier 1 to be the best setup for future experiments. Thus, the next characterisations are performed just for Amplifier 1.

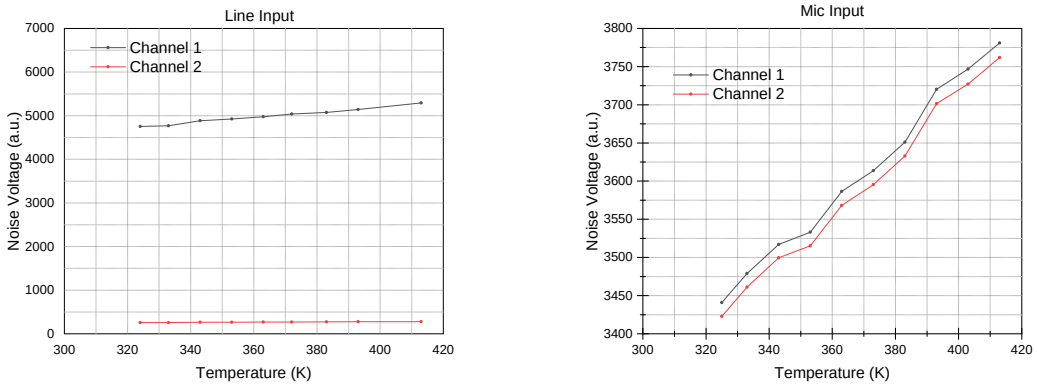

(a) ***Line input*** *(b)* ***Mic input***

Figure 21: ***Comparison of Line and Mic input***

4.5 Change of Noise Figure with Thermal Noise for Amplifier 1

With the change of the thermal noise read by the amplifier, the noise figure of the amplifier will vary as well. This is demonstrated by performing the noise figure detection, discussed before with varying resistors at the input. The resistors are heated as discussed before and the thermal noise voltage is recorded. From the thermal noise voltage, the noise temperature and correspondingly the noise figure is found for the various loads. Figure 22 shows the varying noise figures for Amplifier 1 with varying thermal noise voltage at the input.

Results

Figure 22 shows the noise figure of Amplifier 1 plotted against varying loads at the input. For loads in between the orders of 1 kΩ and 100 kΩ the amplifier is well suited to detect the thermal noise of the resistors quite accurately. This illustrates the range of resistance of the sample which the amplifier can measure well. As discussed before, for loads lesser than 1 kΩ the thermal noise of the resistor is too small to be detected by the amplifier with high sensitivity. For loads greater than the order of 100 kΩ the input resistor of 1 MΩ shown in Figure 9 as well as in Figure 11, suppresses the thermal noise voltage from the input terminals. This results in random fluctuations and a shift in biasing.

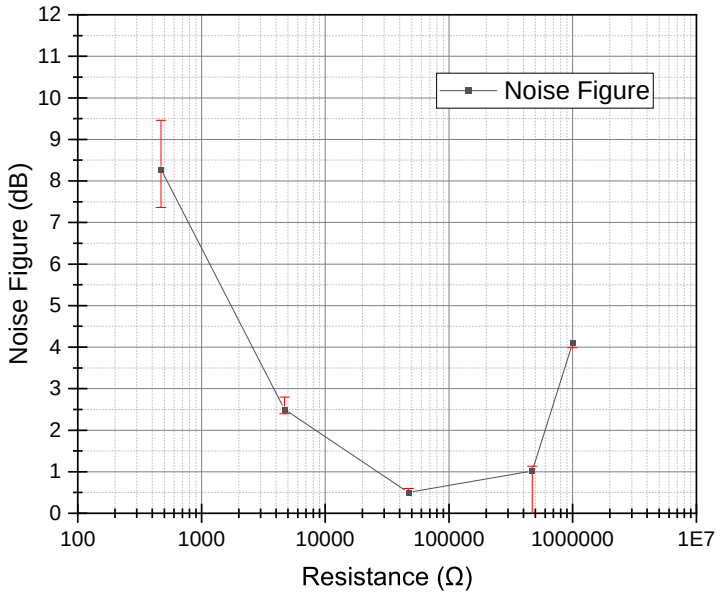

Figure 22: ***Plot of Noise Figure vs. Different Resistances for Amplifier 1***

4.6 Noise Spectrum of Amplifier 1

At the input terminals of the amplifier, a 27 kΩ resistor, doped p-silicon sample (Sample A) and graphite Sample A are attached. The output of the amplifier is seen using a Digital Oscilloscope (DSO). Thermal noise signal is ideally white in nature. Occurrences of 1/f noise and burst noise are possible within the amplifier, which may affect the data while taking the measurements. Thus, observing the spectrum of these samples may help to draw more insights into the behaviour of the sample as well as of the equipment.

The Digital Oscilloscope can perform fast Fourier transform (FFT) on the output of the amplifier. Figure 23 shows the FFT (with Rectangular Window to study the pseudo-random noise impulses) spectrum of the output signal for each of the components at the input.

It can be seen in Figure 23 that for the 27 kΩ and the graphite sample, the spectrum is white. This suggests that 1/f noise may not be present. But for the p-silicon sample, as seen in Figure 23b, around the region of 2 KHz, 1/f noise exists. Upon close observation, occasional occurrences of 1/f noise-alike are also seen for the graphite sample in Figure 23c. However, it is sporadic and lasts only for a short instance which indicates that it might just be external interference affecting the spectrum and not 1/f noise.

Upon hearing the output of the amplifier through a pair of earphones, it is clear that burst noise is evident when the input-load to the amplifier is very small.

The reasons for the 1/f noise may either be from interference with the amplifier itself or directly from the sample at the input. Occurrences of $1/f^n$ in graphene have been studied extensively, e.g. in [33]. Conclusive arguments on these noise sources are challenging to draw due to the nature of this noise. 1/f and $1/f^2$ noise are always possible at the measuring frequency bandwidth but has been generally ignored in the present study until explicitly specified.

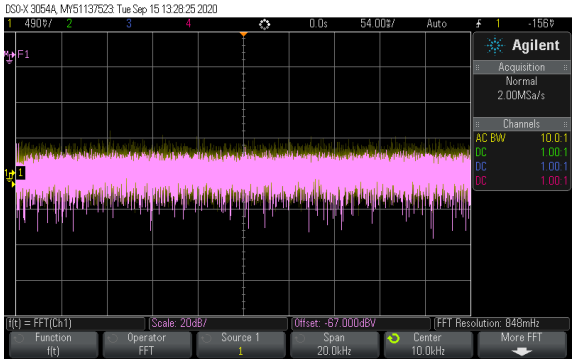

(a) ***FFT on the output spectrum of 27 kΩ resistor from the DSO***

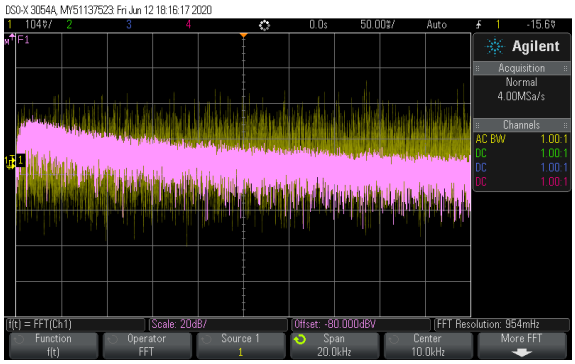

(b) ***FFT on the output spectrum of the doped Si sample from the DSO***

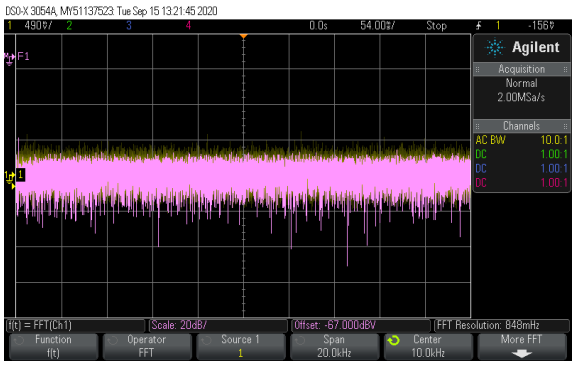

(c) ***FFT on the output spectrum of the Graphite sample from the DSO***

Figure 23: ***Apparent Carrier Temperature in Doped Si Samples, deduced from the magnitude of noise using Amplifier 1***

Once the amplifiers and the input options are characterised, measurements of the silicon and graphite samples, discussed in Chapter 3 are performed with Amplifier 1 connected to the line input. It is also clear that the amplifier imparts some internal noise and thus, the carrier temperatures to be calculated will be influenced by the presence of this noise, i.e. amplifier noise. To eliminate this noise, a correction is performed which is discussed in the following chapter.

5 GENERALISED NOISE MODEL TO ELIMINATE AMPLIFIER NOISE

In the present study to find the temperature of the photo-excited hot carriers generated in the silicon samples discussed so far, the carrier-temperatures are deduced from the first "dark" recording i.e. from the ambient conditions without the illumination of the semiconductor wafer through the lens. But as discussed before, the noise recorded into the computer consists of the noise generated in the sample along with the noise of the equipment.

In this method of determining the temperature of hot carriers, internal noise of the amplifier is subtracted from the net noise read by the computer. Hence, finding the internal noise of the equipment is necessary. The internal noise of equipment is found based upon the noise figures discussed in Chapter 4.

5.1 Equivalent Noise Model of the Amplifier

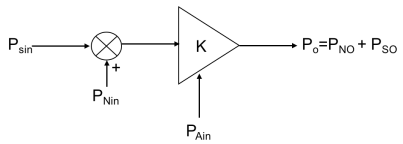

(a) ***Original***

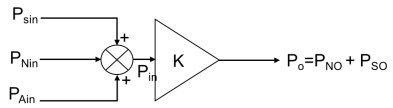

(b) ***Modified***

Figure 24: ***Amplifier Noise Model***

From Figure 24a, P_{sin}, P_{Nin} and P_{Ain} represents the average power of the input voltage signal, noise from the input (the sample or resistor) at the input terminals and noise of the amplifier respectively. The signals are amplified by the amplifier with gain K. P_o represents the average power of output. The output consists of the amplified input signal: P_{so} as well as the amplified noise at the output P_{No}. Signal to noise ratio, SNR is given by:

$$SNR = \frac{P_s}{P_N}$$

where P_s is the power of source signal and P_N is the power of the noise signal. While the noise factor is given by:

$$F = \frac{(SNR)_{in}}{(SNR)_{out}}$$

where $(SNR)_{in}$ is the signal to noise ratio at the input and $(SNR)_{out}$ is the signal to noise ratio at the output.
i.e.

$$F = \frac{P_{sin}}{P_{Nin}} \frac{P_{No}}{P_{so}}$$

The gain K is given by:

$$K = \frac{P_{so}}{P_{sin}}$$

as well as

$$K = \frac{P_{No}}{P_{Nin}}$$

Now if there is no input signal but only noise across the input terminals, the output noise signal is:

$$P_{No} = P_{Aout} + K.P_{Nin}$$

where P_{Aout} is the amplified equipment noise P_{Ain} i.e. P_{Aout} = K.P_{Ain} Thus, the noise figure can be written as:

$$F = \frac{1}{K}(\frac{P_{No}}{P_{Nin}}) = \frac{1}{K}(\frac{P_{Aout} + K.P_{Nin}}{P_{Nin}}) = \frac{1}{K}(\frac{K.P_{Ain} + K.P_{Nin}}{P_{Nin}}) = \frac{P_{Ain} + P_{Nin}}{P_{Nin}} \tag{4}$$

Now Figure 24a can be modified as Figure 24b, where P_{sin}, P_{Nin} and P_{Ain} are taken as independent sources to an ideal amplifier with zero noise factor. Thus, upon considering **only** the noise from the input:

$$P_{in} = P_{Ain} + P_{Nin}$$

where P_{in} is the total input to the amplifier.

Plugging this value into eq. (4):

$$F = \frac{P_{in}}{P_{Nin}}$$

i.e.

$$P_{Nin} = \frac{P_{in}}{F}$$

Finally,

$$P_{in} = P_{Ain} + P_{Nin}$$

which gives

$$P_{Ain} = P_{in} - \frac{P_{in}}{F}$$

$$P_{Ain} = P_{in}(1 - \frac{1}{F}) \tag{5}$$

Thus from eq. (5) the amplifier noise can be deduced. No input signal but only input noise is present in the samples which satisfies the conditions of calculating P_{Ain}. From the noise power recorded originally, the amplifier noise P_{Ain} must be subtracted followed by the steps described in Chapter 3, i.e. the temperature of carriers is deduced using eq. (3).

5.2 Procedure of Finding Carrier Temperature

From Chapter 4, the noise figure of Amplifier 1 is discussed. Thus, the resistance of the sample under illumination helps to determine the noise figure, as seen in Figure 22. This noise figure is used in eq. (5) after calculating the required anti-log calculation to obtain the noise factor.

The following steps are performed to find the carrier temperature from the noise of the amplifier:

1. The voltage equivalent of the sample's noise is obtained as before from section 3.5.
2. The corresponding noise power is obtained by squaring the voltage, still in a.u.
3. The drop in resistance is already available from Table 2 and Table 3. The noise figure of the corresponding resistance under illumination is obtained from Figure 22.
4. The noise factor is obtained by taking the corresponding anti-log.
5. Thus, the noise power of the amplifier is calculated from eq. (5).
6. The noise power of the amplifier is subtracted from the noise power calculated in Step 2 (from both, the "dark" and "concentrated sunlight" noise powers).
7. Using eq. (3) along with the results from Step 6, the carrier temperature is calculated as before by taking the first "dark" reading as the reference.

6 EXPERIMENTS ON EXTRINSIC P-TYPE SILICON

Once the amplifiers are characterised, it is necessary to test the methodology to measure the carrier-temperatures in semiconductors. Undoped and doped silicon chips are mounted on two copper blocks, as discussed in Chapter 3. In this chapter, doped silicon chips A, B, C (discussed in Chapter 3) are tested with Amplifier 1 across the line input following the results of Chapter 4.

Firstly, it is important to measure the change in resistance under illumination through the lens. A digital multimeter (DMM) is attached across the two blocks, as shown in Figure 25. The lens produces a 2 mm bright spot of the sun and the corresponding resistance of the sample is noted when illuminated with this spot.

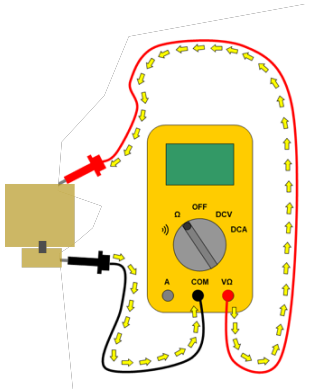

Figure 25: ***Resistance Change Measurement of the samples through a DMM***

Table 2 shows the resistance in ambient conditions as well as under concentrated sunlight. To find the temperature of the photoexcited carriers eq (3) is used. As seen in Table 2 the change of resistance is not significant i.e. $R_{ref} \approx R_T$. Thus eq. (3) becomes:

$$T_{Hot-Carriers} \approx T_{ref} \frac{\overline{V_T^2}}{\overline{V_{ref}^2}}$$

For the main experimental measurements, the steps described in Chapter 3, section 3.5 are performed for all the three samples of doped P-type silicon.

Table 2: ***Change in resistance under illumination for the Doped Si Samples***

Sample	**Resistance in dark (Ohm)**	**Resistance under Concentrated Sunlight (Ohm)**
Sample A	292	289
Sample B	402	379
Sample C	1112	925

Results

Figure 26 illustrates carrier temperatures from the dark measurements and the measurements under concentrated sunlight for each of the doped samples along with the elimination of amplifier noise as discussed in Chapter 5. From Figure 26, it can be seen that the carrier temperatures under illumination decreased compared to the dark most of the times (even negative for one instance).

Firstly, when amplifier noise is not corrected for: Carrier temperatures referred to as "Dark" and "Concentrated Sunlight"

The plot shows the temperature of the carrier deduced from the reference noise under ambient conditions, i.e. from the first "dark" measurement performed in the ambient condition without illumination under the lens. Figure 26 illustrates that in most cases, the temperature of the carriers upon illumination is smaller than that under ambient temperature. The carrier temperature under illumination falls in the range of 250-290 K.

The fall in carrier temperature under illumination can be accounted for from eq (3): $\overline{V_T^2}$ is smaller than $\overline{V_{ref}^2}$. This general trend represents the drop in thermal noise proportionally with the change in the resistance, i.e. increase in photoconductivity. Discussions on this photo-conductivity and the reasons for the drop in temperature below the ambient temperature are discussed at the end of this chapter.

Another argument that can be drawn here: the noise figure discussed in Chapter 4 is very high at the resistance order here. This means that the internal noise of the amplifier affects the thermal noise from the samples.

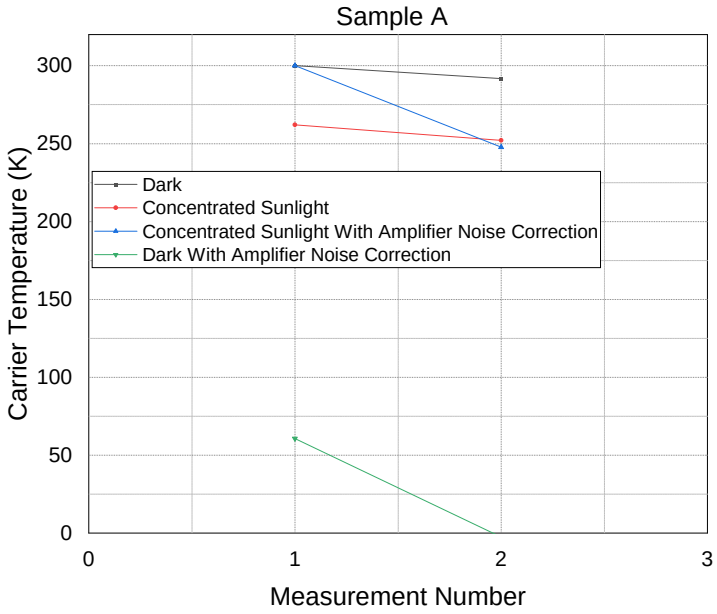

(a) ***Sample A***

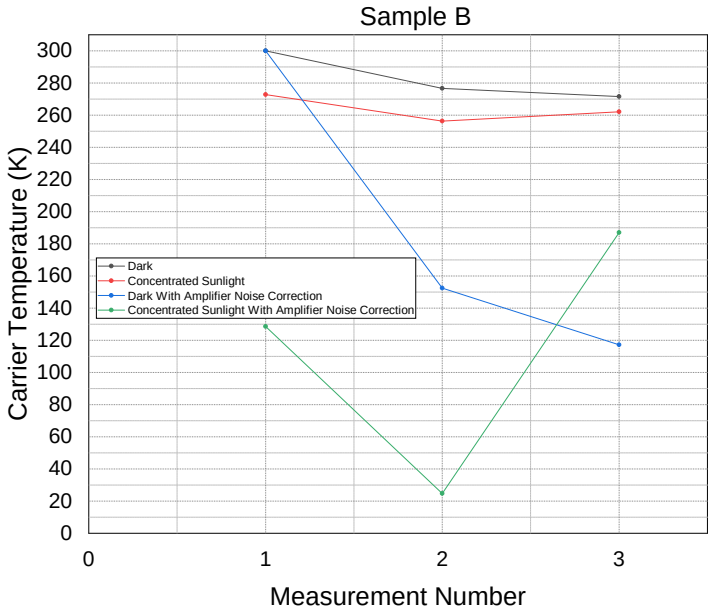

(b) ***Sample B***

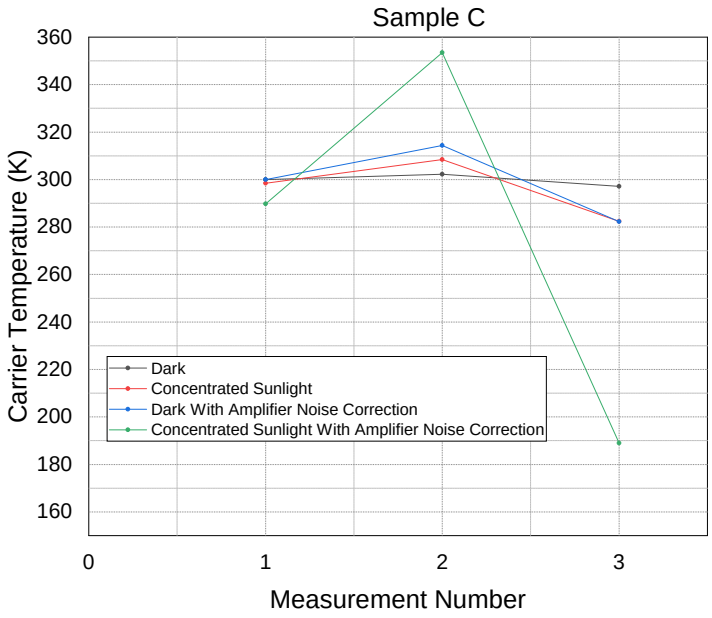

(c) ***Sample C***

Figure 26: ***Apparent Carrier Temperature in Doped Si Samples, deduced from the magnitude of noise using Amplifier 1***

Upon considering the elimination of amplifier noise as discussed in Chapter 5: Carrier temperatures referred to as "Dark With Amplifier Noise Correction" and "Concentrated Sunlight With Amplifier Noise Correction"

The steps discussed above, in section 5.3, are performed on the previously obtained noise voltage power for the doped samples A, B and C. Carrier temperatures corresponding to "Dark With Amplifier Noise Correction" and "Concentrated Sunlight With Amplifier Noise Correction" in Figure 26 shows the carrier temperature of the P-silicon samples, following the steps to eliminate the noise from the equipment. This carrier temperature should have been independent of the noise of the equipment.

The hot-carrier temperatures obtained in this case are in the range of 20-360 K. A significant decrease in carrier temperature below the ambient temperature is witnessed in Figure 26, lower than the results obtained without the amplifier noise correction.

The reason of this behaviour is the equipment noise. The noise figure in the resistance range of the doped samples is above 8 dB as seen in Figure 22. When such a large noise figure is present, it can be argued that the noise of the amplifier has degraded the noise from the sample. The carrier temperatures calculated using eq. (3), after such a large amplifier noise has been subtracted, are very sensitive to the change in the noise powers. Under illumination, as there is a little decrease in the thermal noise of the sample, the recorded temperatures will decrease significantly. And thus, very small carrier temperatures with respect to the reference are obtained through this approach.

The noise temperature of the amplifier for such a high noise figure is enormous. E.g. when the noise figure is around 8 dB, the noise temperature of the amplifier is around 1700 K. Thus, upon subtraction of a large amplifier noise, as well as, a small change in the sample's internal noise under illumination, causes a significantly small carrier temperatures being calculated.

Upon measuring the carrier temperature with high pass filtering and elimination of the amplifier noise, resulting carrier temperatures will be small, even smaller than when amplifier noise is present. This justifies the carrier temperatures obtained in Figure 26. Two distinct behaviours are observed in Figure 26. Firstly, no significant and reproducible rise in carrier temperature is observed under illumination, which signifies that hot-carriers are not observed. Secondly, the correction for amplifier noise causes the carrier temperature to be lower than when amplifier noise is present. Thus, arguments for both these behaviours need to be discussed further.

Conclusion of Experiments on Extrinsic Silicon

Extrinsic Si samples did not show a significant rise in carrier-temperature in the present experiment. Instead, the calculated carrier temperature is close to the ambient temperature. This may be due to the vast pool of cold carriers at the lattice temperature which provides an opposite effect to the photoexcited hot carriers [34]. The noise present is primarily just thermal noise. During illumination through the lens, electron-hole pairs are created, leading to increase in conductivity. Due to this, change in thermal noise is proportional to the decrease in resistance.

The noise generated by the hot e-gas losing its energy to thermal vibrations is subdued due to the vast pool of cold carriers. This may be due to auger-recombination i.e. the excess energy of the hot-carriers are lost to the band-edge states (cold-carriers) instead of any significant phonon modes [34, 35, 36]. Significant increase in carrier temperature is henceforth not witnessed under illumination. The cold carriers remain at the ambient temperature and the only times, an increase in carrier-temperature is witnessed maybe just due to lattice heating. This makes it difficult for hot carriers to be measured in p-doped silicon through this method. The contacts to the sample against copper plates are purely ohmic [37]. This means that there is no electric field or space charge region present inside the samples. Thus, in the absence of a field within the sample and no external bias, the probability of generation-recombination noise is low. Other sources of noise may

be thermal shot noise [38, 22], internal noise of the equipment as well as external factors only.

As discussed from the results of Amplifier 1, another reason for the unreliable data is the internal noise of the equipment. From Table 2, in the resistance range of the samples, the amplifier has a high noise figure, thus resulting in the equipment overpowering the thermal noise signal from the samples. This can be another reason for explaining the fall in carrier temperature under illumination when the thermal noise signal is too weak. It is important to note that this is an example of the limiting condition of the equipment where the noise figure is unstable.

Although it has been attempted to eliminate the effects of the amplifier, the doped samples did not show any hot-carriers. Instead, a fall of temperature below 300 K is recorded through this approach, even lower than, when the noise of the amplifier is present. The subtraction of the amplifier noise has a negative impact on the raw noise signal from the sample because of the high noise figures.

After discussing the limitations of doped silicon samples and analysing the reasons due to which hot carrier temperature could not be measured, it is also interesting to test intrinsic samples. Due to the absence of these free carriers, the resistance of these samples match better with the input impedance of the amplifier, i.e. provides a better load matching and correspondingly better noise figures. Thus, unintentionally doped silicon samples or undoped Si samples are tested next which is discussed in Chapter 7.

7 EXPERIMENTS ON INTRINSIC SILICON

Since doped silicon did not show a significant decrease in resistance or increase in noise under concentrated sunlight, deriving the temperature of hot carriers from doped silicon does not seem very plausible through this approach. Thus, it is also of interest to study the same effect in samples of intrinsic silicon with the same objective of observing and measuring the temperature of hot carriers as there are no free-cold carriers to dilute the photoexcited hot carriers. It is also of interest to differentiate the behaviour of the intrinsic sample against the doped sample in Chapter 6 under illumination.

In Chapter 3, samples of intrinsic silicon (sample A, B) have been discussed. Similarly, as discussed in Chapter 6, the change of resistance under illumination is recorded first. The mounted samples are again connected across a multimeter, as shown in Figure 25.

Table 3 shows the resistance in ambient conditions as well as when the sunlight is focused on the sample forming a 2 mm bright spot. Once the fall in resistance is recorded, the samples are ready for the main experiments.

Table 3: ***Change in resistance under illumination for Undoped Si Samples***

Sample	**Resistance in dark (K Ohm)**	**Resistance under Concentrated Sunlight (K Ohm)**
Sample A	84.5	2.5
Sample B	357	8

Results

Figure 27 shows the plot of the apparent carrier temperature of the e-gas under illumination. The carrier temperature is deduced from the noise power of the initial dark reading using eq. (3). Following the steps described in Chapter 5, the amplifier noise is subtracted from the total noise recorded by the computer.

Firstly, when amplifier noise is not corrected for: Carrier temperatures referred to as "Dark" and "Concentrated Sunlight"

From the DMM, the decrease of resistance under illumination for both the undoped samples is seen in Table 3. Unlike the doped samples, in eq. (3), the resistance change cannot be ignored since the change in resistance is significant. The resistance drop should have produced a decrease in the thermal noise for the samples. But as seen in Figure 27, there is a significant rise in the temperature of the e-gas. Recorded carrier-temperatures are in the range of 20000-200000 K, which are unrealistic. This is due to a massive increase in noise under illumination.

From eq.(3): $\overline{V_{ref}^2}$ is significantly smaller than $\overline{V_T^2}$ under illumination through the lens. It becomes difficult to draw conclusive arguments upon the reasons for such a large increase in noise of the sample. A few predictions of this behaviour are presented later in this chapter under conclusion.

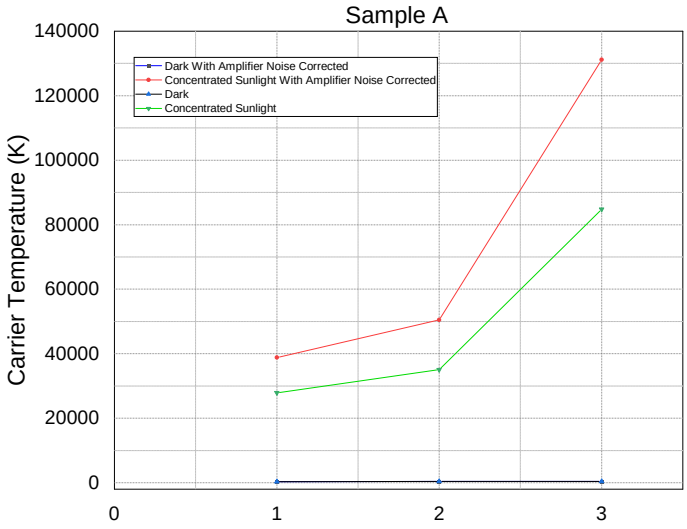

(a) ***Sample A***

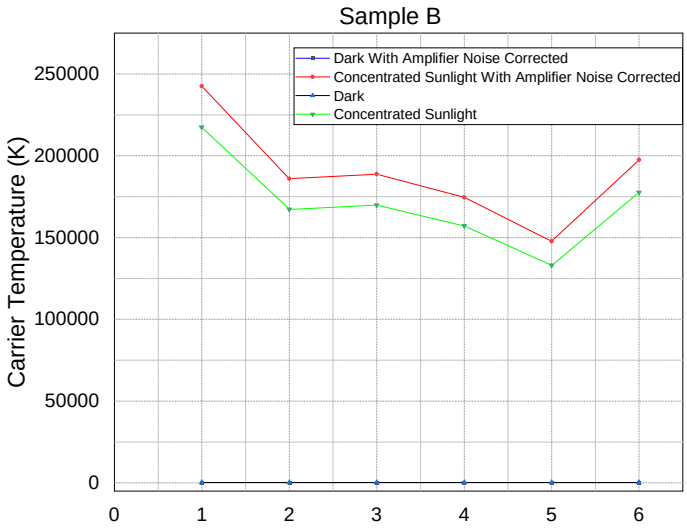

(b) ***Sample B***

Figure 27: ***Apparent Carrier Temperature in Undoped Si Samples, deduced from the magnitude of noise using Amplifier 1***

On the other hand, a rise in the number of photoexcited carriers shows a significant rise in photoconductivity [21, 22]. Thus, R_T is significantly higher compared to R_{ref} under concentrated sunlight. The two ratios in eq. (3) are hence at-least of order 10 each. This makes the $T_{Hot-Carriers}$ in eq. (3) extremely high and unrealistic.

Upon considering the elimination of amplifier noise as discussed in Chapter 5: Carrier temperatures referred to as "Dark With Amplifier Noise Correction" and "Concentrated Sunlight With Amplifier Noise Correction"

The noise figure is calculated from Figure 22. The noise figures in the resistance range of these undoped samples are relatively low, in the range of 2.1 dB for Sample A and 0.5 dB for Sample B. Thus, the amplifier noise corresponding to these noise figures is calculated from the first dark measurements of noise for samples A and B. Clearly, with such low noise figures, the noise induced by the amplifier is small and the noise of the samples does not suffer a significant degradation. The corresponding noise temperature of the amplifier is 180 K when the noise figure is 2.1 dB and 35 K when the noise figure is 0.5 dB, unlike 1700 K seen when the doped silicon samples are measured. An example of calculating the noise of the amplifier and correspondingly finding the carrier temperatures is illustrated in Appendix 1. The carrier temperature calculations for sample A is shown in Table 8.

The amplifier noise is again subtracted from the total noise power of the undoped samples A and B. The carrier temperatures for the undoped samples are again plotted in Figure 27 by following the steps enlisted in section 5.2.

As seen in Figure 27, the carrier temperature is in the range of 40000-250000 K, which is higher than when amplifier noise was not subtracted. This indicates that the model described in Chapter 5, will cause a decrease in noise floor level and results in more accurate results. Unlike the effects seen for the doped Si samples, the subtraction of amplifier noise will provide better results as long as the resistance of the sample leads to small noise figures.

Conclusion of Experiments on Intrinsic Silicon

Thus, in conclusion, the unintentionally doped silicon samples under concentrated sunlight demonstrate reproducible large noise magnitude. The corresponding carrier temperature, i.e. the e-gas temperature falls in the range of 40000 K - 250000 K which is unexpectedly high. Reasons for such large noise magnitude under illumination have not been conclusively found, but rather a few arguments predicting this behaviour have been drawn here. There are two mechanisms which occur within the sample: decrease in resistance due to generation and excitation of electron-hole pair into the conduction band and valence band respectively and the increase in temperature due to increase in the internal noise of the sample.

The large increase in noise under illumination may be accounted for due to noise through the photo-current fluctuations, flux variations at the contacts, thermal noise [22] and the noise at the barriers in the space charge region between the intrinsic chip and the aluminium contact with the copper blocks [39]. The metal-semiconductor is not purely ohmic in this case [40]. Radiative-recombination [41] causing impact-ionisation [42] may be another reason for such large noise under sunlight.

Unlike the doped samples, the vast majority cold carriers are absent for cooling down the highly excited carriers. Shot noise due to photoexcitation and dark current noise can also be present [38]. External sources of noise which is seen as interference are from the mains or any other equipment nearby as well as fluctuation of solar radiation intensity. Discussion on these solar radiation fluctuations is presented later in this study.

On the other hand, the equipment noise has been corrected for in Figure 27. The noise figure is low in the present resistance range. Thus, it can be concluded that subtracting the amplifier noise from the net noise power did not have a significant improvement to the unexpectedly large results because of the large noise magnitude generated within the sample under illumination. However, contrary to the results from when the amplifier noise was present, the carrier temperatures have increased, indicating that the noise floor has reduced upon this subtraction.

In conclusion, as discussed from the results of the samples with Amplifier 1, there is a significant rise in noise within the sample as well as a significant decrease in resistance. The increase in the internal noise of the sample causes a proportional increase in the carrier-temperatures that compensates for the decrease in resistance which is the fundamental idea behind this methodology. Nevertheless, the rise in the sample's internal noise power, as well as drop-in resistance, causes the carrier-temperature to be unexpectedly high, according to eq. (3) due to the two ratios.

Further predictions on the behaviour of silicon are discussed in the "Results and Conclusion", presented at the end of the report. Henceforth it can be argued that finding hot carrier temperature in undoped silicon where a large increase in noise, as well as photoconductivity is observed simultaneously, may not seem possible unless new insights are explored. It still becomes interesting to characterise each of the sources of this large noise magnitude separately or to find an alternative method to measure the accurate temperature of the photo-excited carriers in such intrinsic semiconductor materials. Thus, in the next chapter, intrinsic graphite samples are tested with the present objective.

8 EXPERIMENTS ON GRAPHITE

Once the measurement on silicon samples are complete, the two samples of graphite, discussed in Chapter 3 are tested. The change in resistance is measured, as shown in Figure 25. Table 4 shows the resistance of the samples in the dark and under concentrated sunlight. Similar to the doped samples, the change of resistance is significantly low, i.e. $R_{ref} \approx R_T$. Thus eq. (3) becomes:

$$T_{Hot-Carriers} \approx T_{ref} \frac{\overline{V_T^2}}{\overline{V_{ref}^2}}$$

Table 4: ***Change in resistance under illumination for the Graphite Samples***

Sample	**Resistance in dark (K Ohm)**	**Resistance under Concentrated Sunlight (K Ohm)**
Sample A 23.07.20	60.7	59
Sample A 28.05.20	24.5	24
Sample B	44	40

In Table 4, Sample A is measured on two days, i.e. on 28.05.2020 and 23.07.2020. A change in the dark resistance is obtained. This is because of the rough penciling of the graphite on the rough AlN substrate. The graphite particles do not stick to the substrate well and therefore keep falling off due to friction or due to corrosion while being stored. Thus the resistance of the sample depends upon the amount of graphite transferred during the penciling. The measurements of the carrier temperature are performed for both days.

Following the results of Chapter 4, samples of graphite are only tested with Amplifier 1. As discussed before in Chapter 5, the amplifier noise is again subtracted and the carrier temperatures are thus plotted in Figure 28.

Results

Firstly, when amplifier noise is not corrected for: Carrier temperatures referred to as "Dark" and "Concentrated Sunlight"

After the resistance changes have been measured for both the samples, carrier temperatures are again obtained from the noise recordings, following the procedures enlisted in section 3.5 (in Chapter 3). Figure 28 shows the carrier temperature for Sample A and Sample B. In Figure 28a, measurements of carrier temperatures have been performed on both the days as described above. Clearly, in both the cases of Figure 28a, a significant rise in the carrier temperatures under concentrated sunlight is obtained. The rise in the dark temperature is due to the lattice heating. At the same time, the rise in carrier temperature under illumination may indicate the presence of hot-carriers. Further discussions of this argument are presented in the conclusion section at the end of this chapter. The carrier temperatures obtained under illumination fall in the range of 400-800 K approximately. Whereas when the sun-spot is away from the reference measurement point, as shown in Figure 8, the lattice temperatures are nearer to the ambient temperatures.

Similarly, in Sample B, the carrier temperatures in the dark and under concentrated sunlight show the same trend. In Figure 28b, the carrier temperatures under illumination falls in the range of 360-390 K while when the sun is not focused on the graphite, the lattice temperature is in the range of 300-320 K.

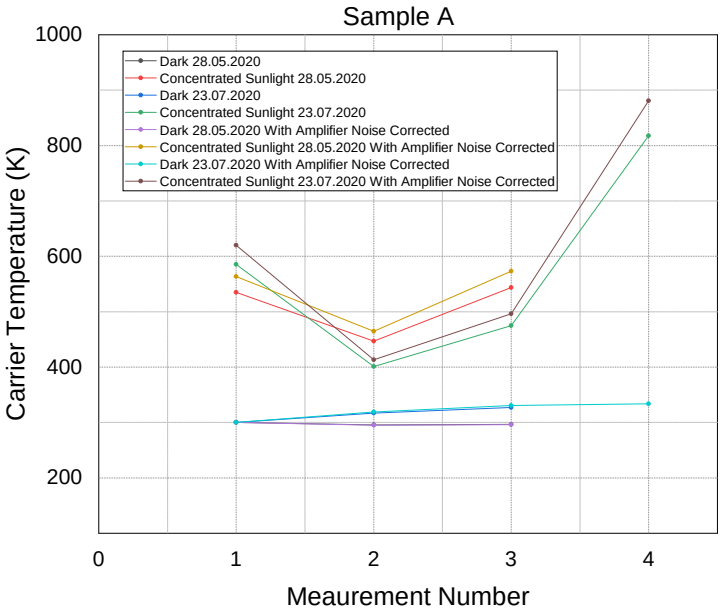

(a) ***Sample A***

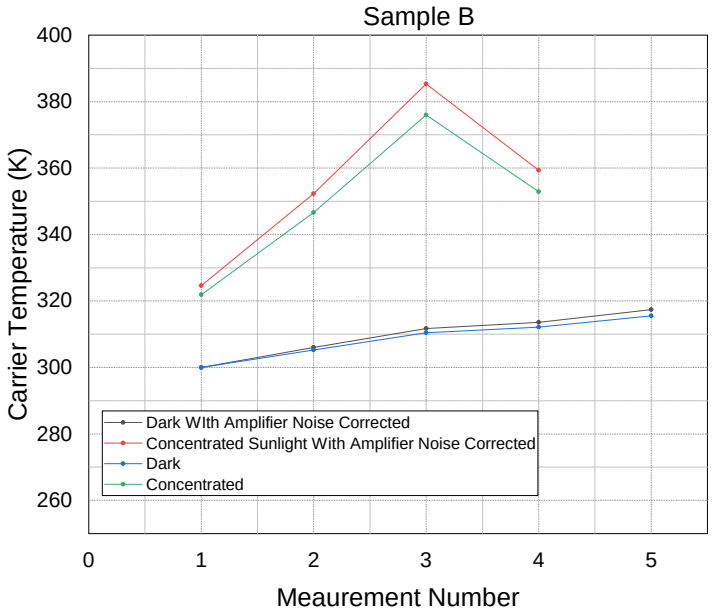

(b) ***Sample B***

Figure 28: ***Apparent Carrier Temperature in Graphite Samples, deduced from the magnitude of noise using Amplifier 1***

Upon considering the elimination of amplifier noise as discussed in Chapter 5: Carrier temperatures referred to as "Dark With Amplifier Noise Correction" and "Concentrated Sunlight With Amplifier Noise Correction"

The resistance change in dark and under concentrated sunlight has been illustrated in Table 4. The corresponding noise figure from Figure 22 is taken to be 0.5 dB. Thus the noise of the amplifier is calculated from the first dark reading and the carrier temperatures are henceforth calculated and plotted in Figure 28. Since the noise figure in the present resistance range is small (0.5 dB), it can be concluded that the amplifier noise for the graphite sample is small and has not significantly degraded the results. Thus, upon subtracting the amplifier noise, a small shift in the carrier temperatures, which can be owed to the effect of equipment noise. The trend seen in the presence of amplifier noise is repeated in after its elimination. Carrier temperatures in the range of 330-900 K under concentrated sunlight are recorded after the elimination of amplifier noise. The increase in the dark carrier temperature is again due to lattice heating as the graphite layer is directly penciled over the AlN substrate.

Conclusion

Under illumination through the lens, a significant rise in the carrier temperature with respect to the lattice is observed in both the cases of Figure 28a and in Figure 28b. The elevated carrier temperatures can be accounted for as hot-carrier temperatures. The increase in the carrier temperature is due to the low free carrier densities (per area) in the thin film of graphite [43, 44] as well as its small bandgap (approx. 40 meV). This results in the photon energy from the sun to be dissipated into a relatively small number of carriers. There is no external bias which may lead to the absence of any generation-recombination noise. Unlike the undoped silicon samples, there exists no space charge region as well. Strong optical absorption, weak screening of the Coulomb potential and high cohesive energy leads to the presence of hot-carriers under strong photoexcitation [43]. Presence of hot-carriers in graphite in the visible and near-infrared region has been studied in [45, 46].

However, there is 1/f noise present as well in the present frequency range as discussed in [33]. In [33], the differences in 1/f noise between graphene and graphite have been studied. Still, as seen in Figure 28, the extent to which the data is affected may not be significant enough. These noise sources should have altered the dark carrier temperatures as well as the carrier temperatures under concentrated sunlight. But evidently, the rise in carrier temperatures in the dark seems to be primarily due to lattice heating, and not due to these noise sources.

The layers of graphite in the samples can be visualised as stacked layers of graphene [47] (ignoring any specific structure formations), even though there are distinct differences between the properties of graphite and graphene. Similar to the results of [48], in the present study, the hot-carriers dominate the photo-response of such intrinsic graphene layers. A similar attempt to find the hot-carrier temperature using Noise Thermometry has been discussed in [44], where average electron temperatures under excitation have been recorded to be in the range of 300-700 K. Carrier-temperatures obtained from Figure 28 reflect similar results. But unlike the present study, the study in [44] is performed using an optical setup and a cryogenic low noise amplifier. Still, based upon the discussions presented yet, it can be argued that the carrier temperatures recorded in Figure 28, does include the temperature of the hot-e gas.

Other mechanism and physical properties of graphite may be present, which affects the results, which still need to be studied further. The carrier temperatures deduced from the recorded noise also include the noise of the amplifier. Thus, developing an alternative methodology which eliminates the amplifier noise becomes necessary. Therefore, following the procedures in Chapter 5, carrier temperatures have been found which are independent of the noise from the amplifier.

Even though no conclusive results were obtained for the silicon samples, the graphite samples showed great potential as an absorber layer and also indicated some success of this method. Advantages and flaws of the setup as well as further discussions of the graphite samples are provided in the Results and Conclusion section at the end of the report. As indicated above, the amplifier noise affects the actual results from the samples and thus, an approach to eliminate the amplifier noise is discussed in the next chapter.

9 ATMOSPHERIC EFFECTS ON SUN'S RADIATION

Atmospheric effects impact the radiation of the sun, which may appear as extra noise on the semiconductor surfaces. It is important to study if these effects make the sun's radiation noisy at the present geographical location for performing any photo-voltaic experiments. Thus, to study this, two independent measurements of the sun's noise, performed simultaneously needs to correlate to each other. The Correlation Coefficient is used as the tool to detect the relation between two such experiments.

The question of whether the sun's radiation at the present location is noisy or not is discussed in this chapter. The setup shown in Figure 29 is used along with the Amplifier 1 shown in Figure 9. However, the two amplifiers of the same are built and connected across channel 1 and channel 2 of the aux input port which connects to the computer. This is illustrated in Figures 29 and 30.

Diodes D1 and D2 shown in Figure 30 are two photodiodes connected in reverse biased across the input terminals of the amplifier. The correlation coefficient of the noise generated by the two photodiodes is used to analyse the effect of the atmosphere. In Figure 30, "$V_o\_Channel\_1$" and "$V_o\_Channel\_2$" are fed to the two inputs of a three-pole aux port, thus forming channel 1 and channel 2.

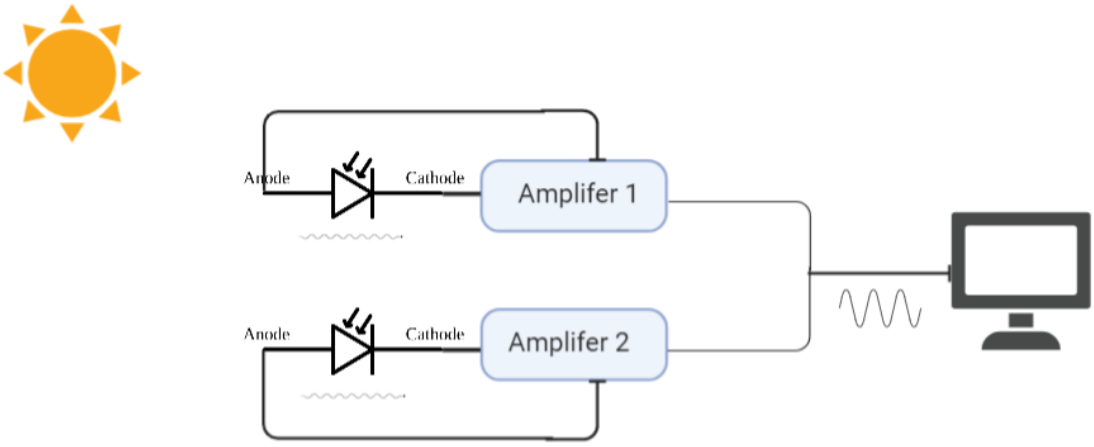

Figure 29: ***Experimental Setup for testing the atmospheric effects on the radiation of sun***

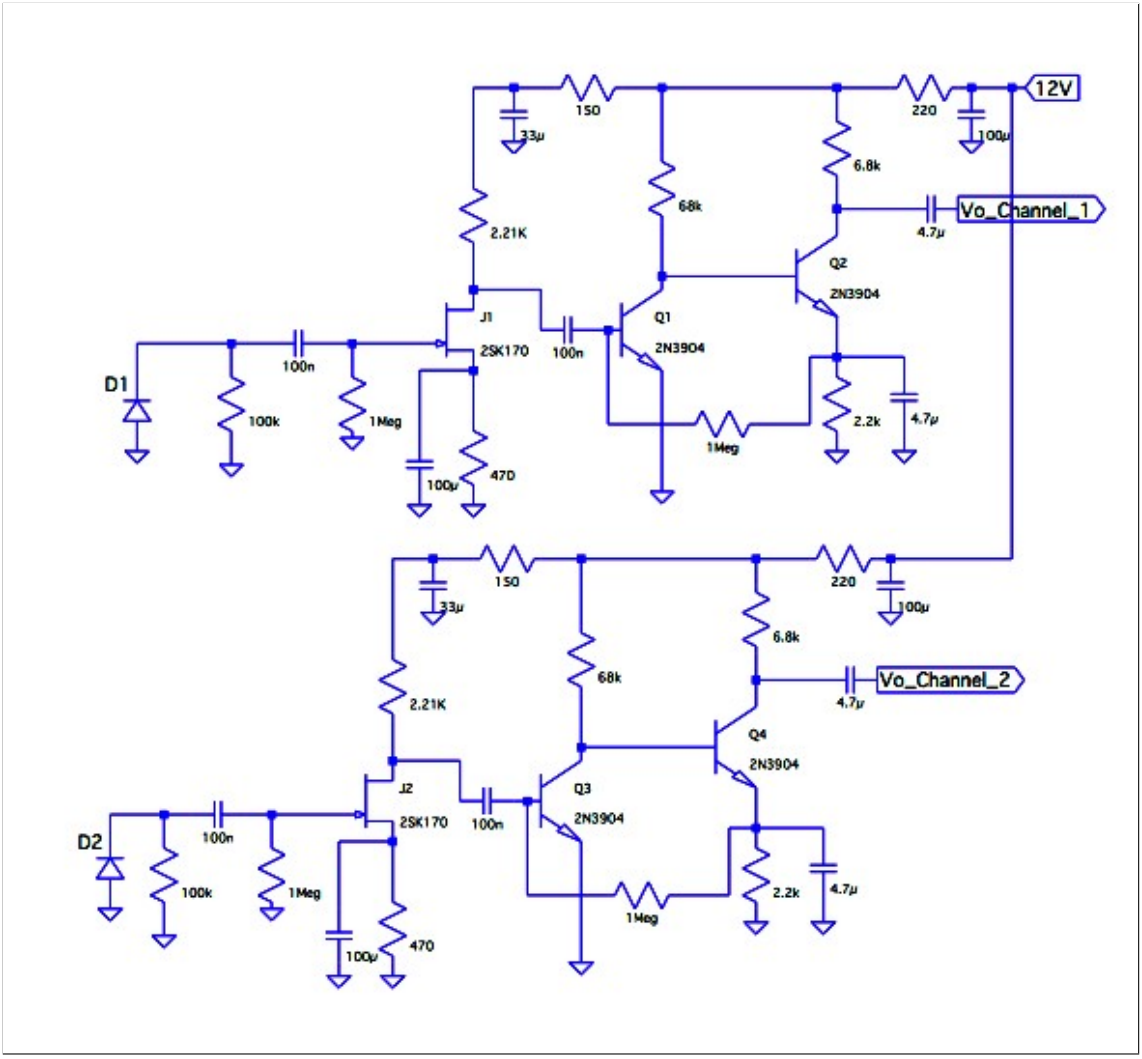

Figure 30: ***Circuit Schematic for testing the Atmospheric Effects on Sun's Radiation***

Correlation coefficient is found from

$$Correl(x,y) = \frac{\sum (x-\overline{x})(y-\overline{y})}{\sqrt{\sum (x-\overline{x})^2 \sum (y-\overline{y})^2}} \tag{9.0}$$

where $\overline{x}$ and $\overline{y}$ are the mean average of set x and y respectively.

Thus, specific to the present experiment, x and y in eq. (9.0) are the data in channel 1 and channel 2. The amplifiers are connected to the line input as the data in channel 1 and channel 2 are needed to be independent of each other, as discussed in Chapter 4.

Once the setup is complete, noise recordings are made using the computer's default audio recording software. The recorded .wav files are treated with a modified version of the C++ program discussed before in Chapter 3. The algorithm of the new program is presented in the form of a flowchart in Figure 31.

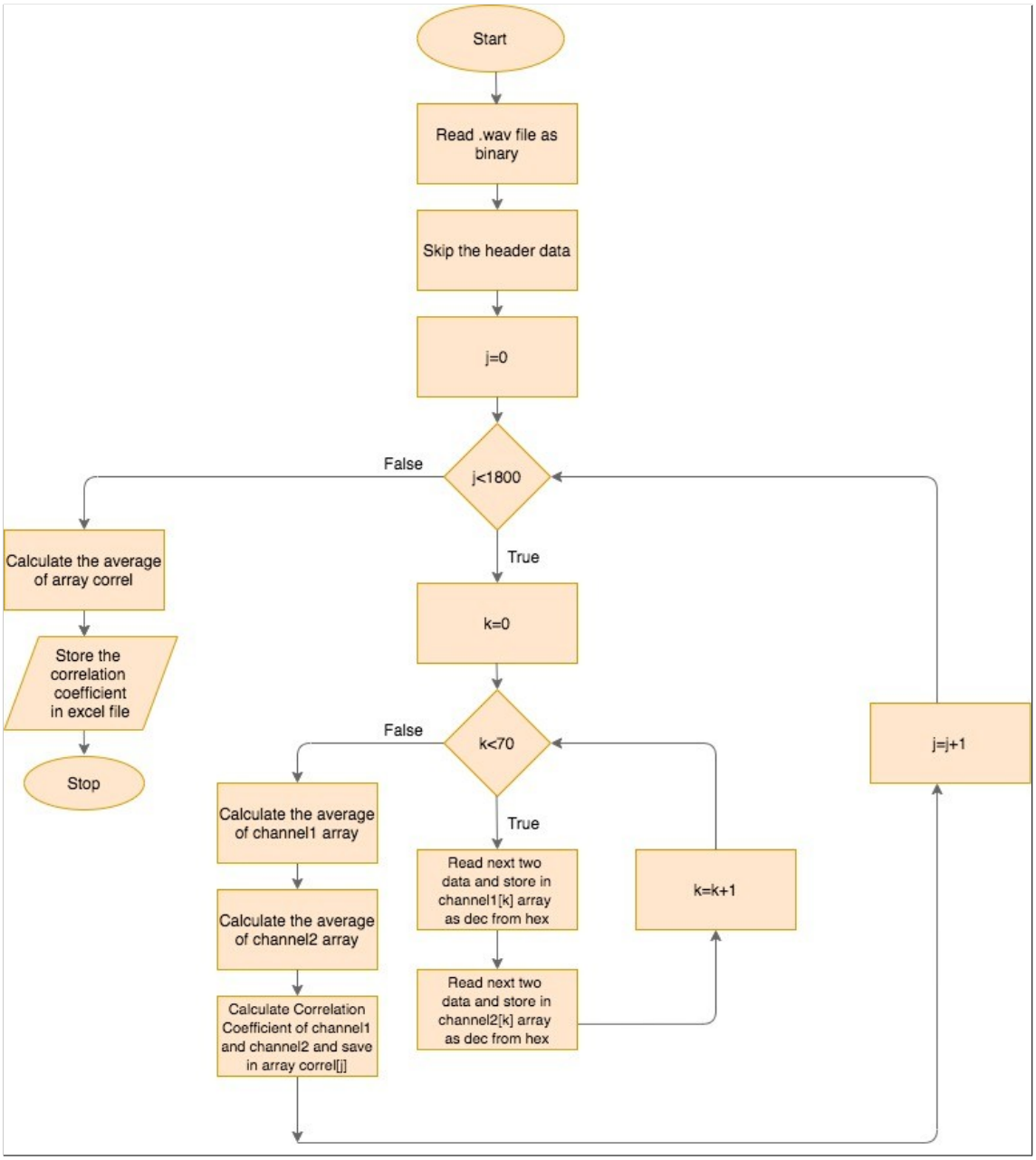

Figure 31: ***Flowchart of the C++ code for finding the correlation coefficient between two channels***

In order to study the effect of the atmosphere on the photodiodes, three cases are tested: 1) dark condition with the photodiodes covered (which is called "dark") 2) illuminated condition light, i.e. in ambient conditions under sun (called "sun") 3) in front of a LED (called "LED") which is operated at 2 KHz and 15 V square-wave signal through a signal generator. Five trials of each of the conditions are performed and the correlation coefficient is thus found between the two channels for all of the 15 cases. Figure 32 shows the plot of the correlation coefficient for each of these three conditions.

Results

From Figure 32, it can be seen that the dark and sun have approximately zero correlation coefficient. While when the LED is placed in front of the photodiodes, the correlation coefficient is nearly 1 or

in other words, positively correlated. This illustrates the idea that under dark or under the sun, the two photodiodes function independently. But when a specific source with a fixed voltage swing is placed in front of the photodiodes, both the photodiodes behave similarly.

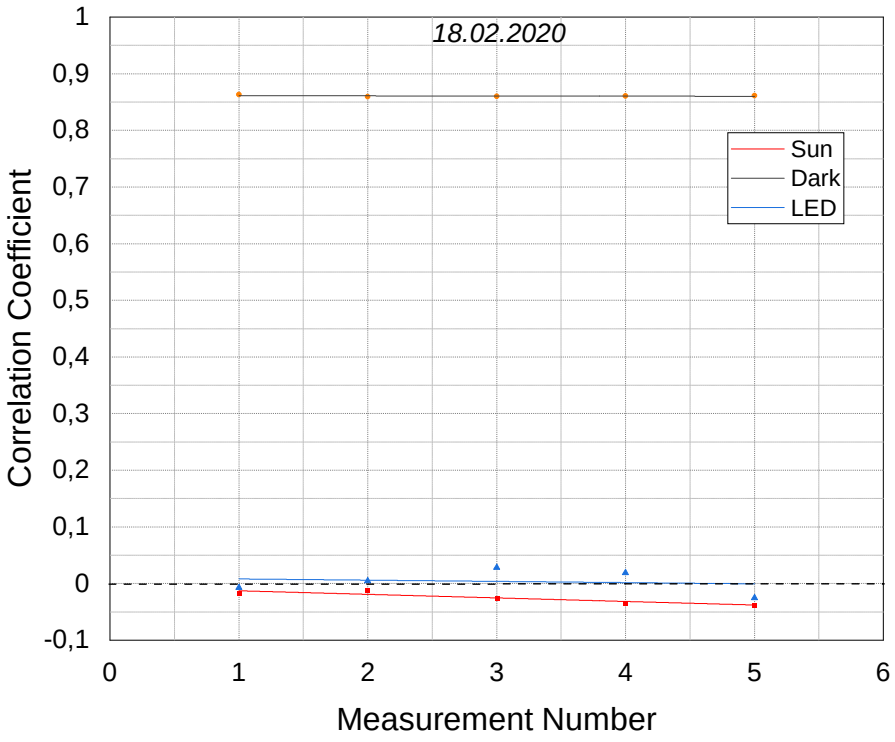

Figure 32: ***Plot of Correlation Coefficient for "dark", "sun" and "LED" to study the effect of radiation of sun***

Hence, it substantiates the idea that when a fixed source is placed in front of the photodiodes, the correlation coefficient between the two will be towards "1" while when there is no fixed source of the noise, the correlation coefficient will be nearly "0". It can be agreed, that since under illumination, the correlation coefficient is nearly zero ("0"), the two photodiodes work independently and the radiations from the sun do not act as a source of noise. It is henceforth concluded that the atmospheric effects do not induce significant and predictable noise in the sun's radiation at the specific location. The atmospheric effects on the sun's radiation can thus be ignored and the sun can be considered "non-noisy".

To study if the argument holds for other days as well, measurements have been conducted on different days for statistical analysis. Figure 33 shows the plot of the correlation coefficient on 21.01.2020 and 31.01.2020. Figure 33a illustrates that the sun and dark measurements of correlation is again nearly zero. In Figure 33b, again, similar trends are obtained as Figure 33a.

Is can be thus concluded from Figure 32 and Figure 33, that under the illumination from the sun, the photodiodes behave similarly when in the dark. Both of the photodiodes behave independently and this proves that the sun doesn't provide a predictable signal source to the photodiodes, i.e. it doesn't act as a significant source of noise for the photodiodes. In conclusion, the external noise due to sun on the samples discussed before and photodiodes can be neglected.

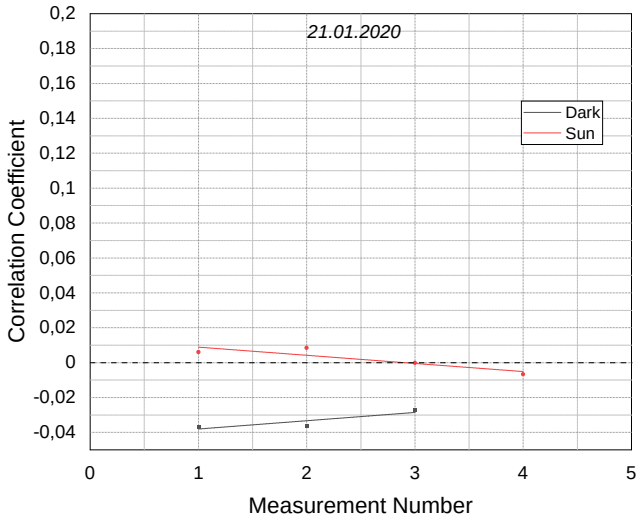

(a) ***Correlation Coefficient on 21.01.2020***

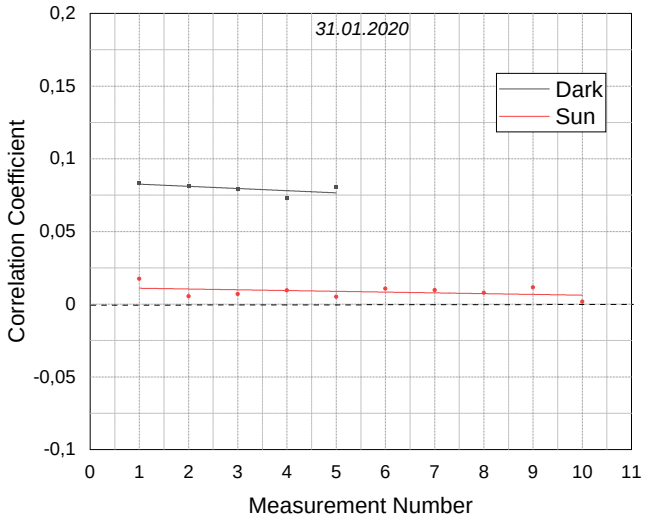

(b) ***Correlation Coefficient on 31.01.2020***

Figure 33: ***Correlation Coefficient on Various days to study the Atmospheric Effects on Sun's Radiation***

RESULTS & CONCLUSION

Measuring the temperature of the hot electron gas is one of the most significant parameters in search of materials which can be used as an absorber layer in the HCSCs. A methodology of finding the temperature of hot-carriers carriers is developed based on the concepts of noise thermometry, as discussed in [18]. In Chapter 4, three amplifiers have been discussed so far. Amplifier 1 showed the best response in measuring thermal noise of loads across the input. Amplifier 2 and Amplifier 3 have been tested to make conclusive arguments that the results of Amplifier 2 and Amplifier 3 are not reliable because of the problems of the mic input. Thus, the results of Amplifier 1 have only been considered.

Amplifier 1 is connected across the line input, which provides better recording possibilities through better noise figures as well as the balance between the two channels. Due to the absence of AGC, the recorded data are not altered. The noise signal read by the amplifier consists of two main sources of noise: noise from the sample and noise from the equipment.

The noise from the equipment consists of the internal noise of the amplifier, atmospheric noise, solar and cosmic noise, noise from the surroundings as well as noise from the main power supply. These noise sources act as interferences during the main experiments. Upon hearing the recorded noise through a pair of headphones, low-frequency noise components, as well as burst noise, have been heard especially when the input load is very small. This is congruent with the noise figure discussed in Chapter 4. As described in [18], there are a lot of factors contributing to the uncertainty in the measurement of noise powers. Amplifier noise is one of the significant contributors. This uncertainty creates inaccuracy in measurements and thus, impacts the results.

The prototype built here is based on the basic principles of Johnson noise thermometry and is similar to the "Switched Rectifier thermometer" discussed in [18]. It is intended to measure the temperature of the noise generated under illumination relative to the reference of the first dark reading. The measurement of noise power includes a combination of the amplifier noise, thermal noise from the connecting wires and the noise from the sample.

For utilising this concept directly, the two noise powers in the "Switched Rectifier thermometer" are made equal, as discussed in [18]. This cannot be done directly in the present study as the noise power with and without illumination vary significantly. An optimal model to calculate the carrier temperature has been discussed, which eliminates the amplifier noise to a great extent.

When the input load is significantly small, the noise signal recorded with the amplifier is not stable anymore, resulting in extremely high noise figures, as seen in Figure 22. Presence of 1/f noise is always a possibility since the measurements are in the audio range. The 1/f noise is thus ignored for the entire course of experimentation and only considered when specified.

Once the amplifiers have been characterised, samples of undoped, doped p-type silicon, as well as graphite are tested. The steps specified in section 3.5 of Chapter 3 have been performed and the results are analysed. The amplifier noise has been calculated and subtracted from the total average noise power of the samples following the procedures enlisted in Chapter 5. The carrier temperature is calculated from the resulting noise power using the eq. (3).

The noise read from the sample may consist of a combination of thermal noise, shot noise, noise from the space charge region and generation-recombination noise. Thermal Noise is the only noise which is intended to be read. Generation and recombination noise may be an effect of thermal noise [22] in the intrinsic silicon samples and conditions of detecting the hot-carrier noise against the g-r noise (in the presence of an electric field) is specified in [22].

Firstly, doped P-type silicon samples have been tested. P-type silicon shows photoconductivity, but it is not very significant for the specific samples used in the present study. The reasons for the photoconductivity has been argued to be the increase in carrier concentration while the rise of temperature has been suppressed, i.e. as observed, the carriers remained near the lattice temperature or correspondingly remained "cold". As discussed in Chapter 6, the samples showed a decrease in noise corresponding to the decrease in resistance. The vast pool of majority carriers due to doping may cause the thermalisation and scattering of hot carriers at the band-edge rather than as phonon-scattering. A significant increase in carrier-temperature is henceforth not observed. The few times an increase in the carrier temperature is witnessed may be due to heating of the lattice only.

Also, in the resistance order of the doped samples, the amplifier has very high noise figure. The noise figures corresponding to the resistance of these doped samples indicate that the internal noise of the amplifier have completely degraded the thermal noise from the samples. This is seen from the model proposed in Chapter 5, after which subtracting the amplifier noise, results in carrier temperatures that are even smaller compared to when amplifier noise was present.

Contrary to the doped P-silicon samples, the undoped samples showed a large increase in the photoconductivity. However, opposite to the drop in resistance, a large increase in noise is also obtained. This increase in noise magnitude and the decrease in resistance results in unexpectedly high carrier temperature obtained from eq. (3). The reasons for the large noise magnitude have not been conclusively found. Nevertheless, assumptions of such behaviour have been discussed in Chapter 7. To recapitulate: the reproducible, large increase in noise under illumination may be due to noise from photo-current and flux fluctuations at the contacts, thermal noise, noise from the space charge region between the intrinsic chip and the copper blocks as well as shot noise. Similar discussions are presented in [22]. It is also possible that a photo-voltage develops across the contacts leading to a possibility of generation-recombination noise. Still the accurate reasons for such a large increase in noise under illumination are yet to be found.

Silicon having a large bandgap makes it a challenge to detect hot carriers generated within the samples. This large bandgap results in poor absorption of the sun's complete spectrum [49, 50]. Crystal defects within the samples and surface impurities may also be present in the samples. Surface impurities, as well as defects within the samples, may generate trap centres of varying lifetimes [51]. This causes a fall in photoresponse and decrease in efficiencies [52, 53, 51]. But in general, the presence and effects of defects in the present study have been ignored. Still, insights into the behaviour and limitations of pure silicon samples as potential absorber layers in HCSC (doped or undoped) have been illustrated in the present report.

Finally, samples of graphite deposited manually on Aluminium Nitride substrate has been measured. The results of the carrier temperatures under illumination, as discussed in Chapter 8, shows the presence of hot-carriers. In the conclusion section of Chapter 8, the argument of the carrier temperature being from hot-carriers has been drawn based upon the results from previous other studies. Graphite shows similarities to graphene which have been confirmed to show hot-carriers [47, 43, 45, 46, 48, 44]. In the absence of any fields probability of generation-recombination noise is low. Other noise sources may include shot noise within the sample [54], 1/f noise [55] as well as external noise from the mains. However, drawing conclusive arguments on the possibilities of these noise sources needs further study of the sample. However, looking at the results of the carrier temperatures in the dark, it does seem that the other noise sources may not have a very significant effect. One of the sources of error may be the contamination of the graphite layers, which might affect the bandgap or the work-function of the deposited layer [56]. Nevertheless, the results of the graphite samples from Chapter 8 does indicate the success of the present methodology. It also defines the working conditions, under which the approach results in successful measurements of hot-carrier temperatures.

As seen from the results of the silicon and graphite samples, the approach described in Chapter 5 may result in success in observing and measuring hot-carrier temperatures. Unlike the bulk doped p-Si samples, a vast pool of majority-free carriers per area unit in graphite is absent, which is a key parameter differentiating the results seen between them. Therefore, samples of any material with low free charge density per area unit and high resistance in the order of 10-400 KΩ seem to suit best for this methodology. Building a sample template with copper/graphite contacts on AlN glued with a copper plate (using thermal glue/paste) seems to be a good sample holder where the required material under test can be deposited between the two contacts, as seen for the graphite samples in the present study. AlN on copper plates is sufficient as a heat sink to be able to keep the lattice cool. This can be seen from the results of Figure 34 discussed in Appendix 2. It is also important that unlike the undoped Si samples, a diode(p-i) like structure is not created. An extreme change in photoconductivity will result in unexpectedly high carrier temperatures, according to eq. (3), as seen for the undoped Si samples.

Finally using this method, the effects of the atmosphere on the sun's radiations has been analysed in Chapter 9 and the conclusive results say that these effects have a negligible influence on the sun's radiations.

Although the silicon samples did not show acceptable results through this approach, it specified which samples are not suitable for this approach. Whereas graphite with an effective heat dissipation path did highlight some success. To draw complete credibility of this approach, additional materials need to be investigated. This method should be further improved to overcome the problems within the equipment and decrease the constraints in selecting the materials to be tested. This leads to vast future possibilities and awaits further experimentations in the future.

FUTURE OUTLOOK

The methodology discussed so far has been tested only for silicon and graphite. Samples of doped p-type silicon and undoped silicon have shown unsuccessful results while the results of graphite show positive results. Thus, based on only a small number of materials under test, drawing complete credibility of the methodology is not possible. It has been predicted that observing hot carrier dynamics for large-bandgap semiconductors such as silicon does not seem to be plausible through this. Materials such as Lead Sulphide, Lead Telluride, Halide perovskites or even hetero-structures with silicon substrate are potential materials that may show higher probabilities of measuring hot carrier temperatures through this prototype. Hence to prove the sustainability of the concept, further experimentations are required with new materials.

In the present study, the lens and the samples were hand-held during the measurements. To study different dynamics of photo-response, a mounting setup for the lens and the samples must be built, especially to make conclusive arguments on aberrations, angle of inclination and the working distance between the lens and the sample.

For the equipment, Amplifier 1 has shown the best response compared to all the other amplifiers tested. However, the limiting condition of this amplifier is the load across the input terminals. As discussed in Chapter 4, Amplifier 1 has better noise figure for loads between 1 kΩ and 100 kΩ order. Thus, new samples must match this order of resistance for better results along with a good heat-dissipation mechanism. Adding a coupling transformer between the stages of the amplifier will result in better resistance matching between the sample and the amplifier especially if the sample has a low resistance such as the doped samples discussed in the present study.

Higher frequency measurements at 3.4 GHz has been predicted. But weak skin effects have proved to be a limiting factor in developing this idea further. Limiting the bandwidth to a higher frequency, such as 100 KHz could result in some better results. At higher frequencies than the present study, the effects of external interference, as well as the effects of 1/f noise, may reduce significantly. 1/f and $1/f^2$ noise have been ignored so far. However, they are still present and affects the actual results. Thus, adding band-limiting filters as well as shifting the operating frequency higher, may give in better results.

Based on other methodologies discussed in [18], the prototype can be developed further to decrease the amount of uncertainty. One such idea would be from the concept of the "Switched Cross-Correlator" (discussed in the same paper). It would be a modification to the present setup and would eliminate the noise from the connecting wires as well as there would be a decrease in the effect of the amplifier noise.

New methodologies and modifications have their problems and thus, vast opportunities and potential of further research still prevail. This concept of extending Johnson Noise thermometry to measure temperatures of hot carriers holds a lot of possibilities, especially evident from graphite. A prototype of the idea, in the audio frequency range, has been proposed in the present study and hopefully will pave paths for a lot of future developments.

BIBLIOGRAPHY

[1] J. Shah, "Hot electrons and phonons under high intensity photoexcitation of semiconductors," *Solid-State Electronics*, vol. 21, no. 1, pp. 43 – 50, 1978.

[2] C. S. Sapp, "Wave pcm soundfile format." `http://soundfile.sapp.org/doc/WaveFormat/`.

[3] W. Shockley and H. J. Queisser, "Detailed balance limit of efficiency of p-n junction solar cells," *Journal of Applied Physics*, vol. 32, no. 3, pp. 510–519, 1961.

[4] A. D. Vos, "Detailed balance limit of the efficiency of tandem solar cells," *Journal of Physics D: Applied Physics*, vol. 13, pp. 839–846, may 1980.

[5] K. Sharma, V. Sharma, and S. S. Sharma, "Dye-sensitized solar cells: Fundamentals and current status," *Nanoscale Research Letters*, vol. 13, p. 381, Nov 2018.

[6] N.-G. Park, "Perovskite solar cells: an emerging photovoltaic technology," *Materials Today*, vol. 18, no. 2, pp. 65 – 72, 2015.

[7] K. E. Jasim, "Quantum dots solar cells," *Solar Cells-New Approaches and Reviews*, pp. 303–331, 2015.

[8] P. Würfel, "Solar energy conversion with hot electrons from impact ionisation," *Solar Energy Materials and Solar Cells*, vol. 46, no. 1, pp. 43 – 52, 1997.

[9] G. Conibeer, J.-F. Guillemoles, F. Yu, and H. Levard, "Hot carrier solar cells," *RSC Energy and Environment Series*, vol. 2014, pp. 379–424, 01 2014.

[10] G. Conibeer, C.-W. Jiang, D. König, S. Shrestha, T. Walsh, and M. Green, "Selective energy contacts for hot carrier solar cells," *Thin Solid Films*, vol. 516, no. 20, pp. 6968 – 6973, 2008. Proceedings on Advanced Materials and Concepts for Photovoltaics EMRS 2007 Conference, Strasbourg, France.

[11] I. Konovalov and B. Ploss, "Modeling of hot carrier solar cell with semi-infinite energy filtering," *Solar Energy*, vol. 185, pp. 59 – 63, 2019.

[12] G. Conibeer, S. Shrestha, S. Huang, R. Patterson, H. Xia, Y. Feng, P. Zhang, N. Gupta, M. Tayebjee, S. Smyth, *et al.*, "Hot carrier solar cell absorbers: materials, mechanisms and nanostructures," in *Next Generation Technologies for Solar Energy Conversion V*, vol. 9178, p. 917802, International Society for Optics and Photonics, 2014.

[13] T. Holstein, "Theory of transport phenomena in an electron-phonon gas," *Annals of Physics*, vol. 29, no. 3, pp. 410 – 535, 1964.

[14] D. J. Farrell, Y. Takeda, K. Nishikawa, T. Nagashima, T. Motohiro, and N. J. Ekins-Daukes, "A hot-carrier solar cell with optical energy selective contacts," *Applied Physics Letters*, vol. 99, no. 11, p. 111102, 2011.

[15] C. Ng, J. J. Cadusch, S. Dligatch, A. Roberts, T. J. Davis, P. Mulvaney, and D. E. Gómez, "Hot carrier extraction with plasmonic broadband absorbers," *ACS Nano*, vol. 10, no. 4, pp. 4704–4711, 2016. PMID: 26982625.

[16] S. Kahmann and M. A. Loi, "Hot carrier solar cells and the potential of perovskites for breaking the shockley–queisser limit," *J. Mater. Chem. C*, vol. 7, pp. 2471–2486, 2019.

[17] H. Nyquist, "Thermal agitation of electric charge in conductors," *Phys. Rev.*, vol. 32, pp. 110–113, Jul 1928.

[18] J. F. Qu, S. P. Benz, H. Rogalla, W. L. Tew, D. R. White, and K. L. Zhou, "Johnson noise thermometry," *Measurement Science and Technology*, vol. 30, p. 112001, sep 2019.

[19] J. P. Nougier, "Identity between spreading and noise diffusion coefficients for hot carriers in semiconductors," *Applied Physics Letters*, vol. 32, no. 10, pp. 671–673, 1978.

[20] T. Sjodin, C.-M. Li, H. Petek, and H.-L. Dai, "Ultrafast transient grating scattering studies of carrier dynamics at a silicon surface," *Chemical Physics*, vol. 251, no. 1, pp. 205 – 213, 2000.

[21] A. M. Musaev, "Effects of local photoexcitation of high-concentration charge carriers in silicon," *Semiconductors*, vol. 51, no. 10, pp. 1290–1294, 2017.

[22] R. Müller, "Generation-recombination noise," in *Noise in Physical Systems* (D. Wolf, ed.), (Berlin, Heidelberg), pp. 13–25, Springer Berlin Heidelberg, 1978.

[23] D. F. Swinehart, "The beer-lambert law," *Journal of Chemical Education*, vol. 39, no. 7, p. 333, 1962.

[24] F. Gibelli, L. Lombez, and J.-F. Guillemoles, "Two carrier temperatures non-equilibrium generalized planck law for semiconductors," *Physica B: Condensed Matter*, vol. 498, pp. 7 – 14, 2016.

[25] M. B. Price, J. Butkus, T. C. Jellicoe, A. Sadhanala, A. Briane, J. E. Halpert, K. Broch, J. M. Hodgkiss, R. H. Friend, and F. Deschler, "Hot-carrier cooling and photoinduced refractive index changes in organic–inorganic lead halide perovskites," *Nature Communications*, vol. 6, p. 8420, Sep 2015.

[26] C. Poole and I. Darwazeh, "Chapter 14 - low-noise amplifier design," in *Microwave Active Circuit Analysis and Design* (C. Poole and I. Darwazeh, eds.), pp. 475 – 517, Oxford: Academic Press, 2016.

[27] K. Seeger, *Semiconductor physics*. Springer Science & Business Media, 2013.

[28] F. Hooge, "1/f noise," *Physica B+C*, vol. 83, no. 1, pp. 14 – 23, 1976.

[29] M. J. M. J. Buckingham, *Noise in electronic devices and systems*. Chichester [West Sussex, England] : E. Horwood ; New York : Halsted Press, 1983.

[30] "Noise in amplifier." `https://www.tutorialspoint.com/amplifiers/noise_in_amplifiers.htm`.

[31] K. Technologies, "Noise figure measurement accuracy – the y-factor method," Sep 2010.

[32] Q. Sun, C. Zhang, W. Shao, and X. Li, "Photodetection by hot electrons or hot holes: A comparable study on physics and performances," *ACS omega*, vol. 4, pp. 6020–6027, Mar 2019. 31459749[pmid].

[33] G. Liu, S. Rumyantsev, M. S. Shur, and A. A. Balandin, "Origin of 1/f noise in graphene multilayers: Surface vs. volume," *Applied Physics Letters*, vol. 102, no. 9, p. 093111, 2013.

[34] T. R. Hopper, A. Gorodetsky, A. Jeong, F. Krieg, M. I. Bodnarchuk, M. Maimaris, M. Chaplain, T. J. Macdonald, X. Huang, R. Lovrincic, M. V. Kovalenko, and A. A. Bakulin, "Hot carrier dynamics in perovskite nanocrystal solids: Role of the cold carriers, nanoconfinement, and the surface," *Nano Letters*, vol. 20, no. 4, pp. 2271–2278, 2020.

[35] K. Rahmat, "Simulation of hot carriers in semiconductor devices," 04 2007.

[36] M. Green, J.-F. Guillemoles, and T. Schmidt, "Project " hot carrier solar cell : Implementation of the ultimate pv converter " final report april," 2009.

[37] S. S. Li, *Metal–Semiconductor Contacts*, pp. 284–333. New York, NY: Springer New York, 2006.

[38] R. Hui, "Chapter 4 - photodetectors," in *Introduction to Fiber-Optic Communications* (R. Hui, ed.), pp. 125 – 154, Academic Press, 2020.

[39] E. L. Kollberg, H. Zirath, and A. Jelenski, "Temperature-variable characteristics and noise in metal - semiconductor junctions," *IEEE Transactions on Microwave Theory and Techniques*, vol. 34, no. 9, pp. 913–922, 1986.

[40] F. Omnes, *Introduction to Semiconductor Photodetectors*, ch. 1, pp. 1–14. John Wiley & Sons, Ltd, 2010.

[41] G. P. Agrawal and N. K. Dutta, *Recombination Mechanisms in Semiconductors*, pp. 74–146. Boston, MA: Springer US, 1993.

[42] K. Misiakos and D. Tsamakis, "Accurate measurements of the silicon intrinsic carrier density from 78 to 340 k," *Journal of Applied Physics*, vol. 74, no. 5, pp. 3293–3297, 1993.

[43] S. Tan, A. Argondizzo, C. Wang, X. Cui, and H. Petek, "Ultrafast multiphoton thermionic photoemission from graphite," *Phys. Rev. X*, vol. 7, p. 011004, Jan 2017.

[44] A. C. Betz, S. H. Jhang, E. Pallecchi, R. Feirrera, G. Fève, J. M. Berroir, and B. Plaçais, "Supercollision cooling in undoped graphene," 2012.

[45] T.-W. Hsieh and C.-W. Lai, "Hot carriers, phonons and electron-phonon decoupling in graphite," in *APS March Meeting Abstracts*, vol. 2013 of *APS Meeting Abstracts*, p. Z5.001, Mar. 2013.

[46] B. Pandit Chhetri, S. Singh, J. Holt, E. Olejnik, Z. V. Vardeny, A. Kirakosyan, and T. Shabazyan, "Ultrafast Spectroscopy of Hot Carriers in Graphite," in *APS March Meeting Abstracts*, vol. 2010 of *APS Meeting Abstracts*, p. Z22.013, Mar. 2010.

[47] A. García-Ruiz, S. Slizovskiy, M. Mucha-Kruczyński, and V. I. Fal'ko, "Spectroscopic signatures of electronic excitations in raman scattering in thin films of rhombohedral graphite," *Nano Letters*, vol. 19, no. 9, pp. 6152–6156, 2019. PMID: 31361497.

[48] N. M. Gabor, J. C. Song, Q. Ma, N. L. Nair, T. Taychatanapat, K. Watanabe, T. Taniguchi, L. S. Levitov, and P. Jarillo-Herrero, "Hot carrier-assisted intrinsic photoresponse in graphene," *Science*, vol. 334, pp. 648–652, Nov 2011.

[49] M. A. Green, "Self-consistent optical parameters of intrinsic silicon at 300k including temperature coefficients," *Solar Energy Materials and Solar Cells*, vol. 92, no. 11, pp. 1305 – 1310, 2008.

[50] M. A. Green and M. J. Keevers, "Optical properties of intrinsic silicon at 300 k," *Progress in Photovoltaics: Research and Applications*, vol. 3, no. 3, pp. 189–192, 1995.

[51] J. R. Davis, A. Rohatgi, R. H. Hopkins, P. D. Blais, P. Rai-Choudhury, J. R. McCormick, and H. C. Mollenkopf, "Impurities in silicon solar cells," *IEEE Transactions on Electron Devices*, vol. 27, no. 4, pp. 677–687, 1980.

[52] W.-J. Yin, T. Shi, and Y. Yan, "Unusual defect physics in ch3nh3pbi3 perovskite solar cell absorber," *Applied Physics Letters*, vol. 104, no. 6, p. 063903, 2014.

[53] K. Arafune, T. Sasaki, F. Wakabayashi, Y. Terada, Y. Ohshita, and M. Yamaguchi, "Study on defects and impurities in cast-grown polycrystalline silicon substrates for solar cells," *Physica B-condensed Matter - PHYSICA B*, vol. 376, pp. 236–239, 04 2006.

[54] L. DiCarlo, J. R. Williams, Y. Zhang, D. T. McClure, and C. M. Marcus, "Shot noise in graphene," *Physical Review Letters*, vol. 100, Apr 2008.

[55] M. Mihaila, D. Ursutiu, and I. Sandu, "Electron-phonon coupling as the source of 1/f noise in carbon soot," *Scientific Reports*, vol. 9, p. 947, Jan 2019.

[56] A. Knápek, M. Horacek, J. Chlumská, T. Kuparowitz, D. Sobola, and J. Sikula, "Preparation and noise analysis of polymer graphite cathode," *Metrology and Measurement Systems*, vol. 25, pp. 451–458, 10 2018.

APPENDIX 1

Conversion Factor between μV and nV for Amplifier 1

The thermal voltage recorded by the amplifier is presented in arbitrary units. To convert this a.u. of voltage into standard nV, the following steps are performed:

1. A resistor at the input is heated and the noise temperature is found, as discussed while finding the noise figure of the amplifier.
2. The arbitrary units of the voltage recorded are squared to find the corresponding noise power.
3. As before, the curve of the recorded noise power is plotted against the temperature of measurements. From the intercept of the curve with the X-axis, the 0 K noise power is calculated.
4. This 0 K noise power is subtracted from the recorded noise power in 3.
5. The square root of the results obtained from Step 4. provides the thermal noise voltage. The ratio of this thermal noise voltage with the arbitrary noise voltage which is initially recorded provides the required conversion factor for each of the temperature points where noise has been recorded.
6. The average of all the conversion factors for each of the temperature points provides the net conversion factor between a.u. and nV. for the. corresponding resistance.

The net conversion factor is found for all the resistors which are used to determine the change in noise figure, as discussed in Chapter 4. Table 5 illustrates the conversion factor for the various resistors at the input. From Table 5, the average conversion factor is 2.077. Thus, V (nV) = 2.077 * V (a.u.)

Table 5: ***Conversion Factor between a.u. and nV of Amplifier 1***

Resistance (Ohm)	Conversion Factor
470	1.993
4700	2.069
47000	2.137

Example Calculations

Measurement of Noise Figure and Noise Temperature

In Chapter 4, the noise figure and noise temperature of Amplifier 1 with a load of 47 kΩacross the input is found. Table 6 shows the recorded noise voltage against the temperatures of measurement. Column 3 consists of the noise power obtained by squaring the noise voltage recorded. Figure 15b shows the plot of this noise power plotted against the temperature in K.

Table 6: ***Calculation of Noise Figure for Amplifier 1***

Temperature (°C)	**Noise Recorded (a.u.)**	**Noise Power = Noise Recorded^2 (a.u.)**	**Temperature (K)**
140	2248,44	5055482,434	413
127	2221,72	4936039,758	400
120	2200,42	4841848,176	393
110	2177,44	4741244,954	383
100	2153,75	4638639,063	373
90	2137,63	4569462,017	363
80	2096,79	4396528,304	353
70	2062,19	4252627,596	343
65	2054,09	4219285,728	338
60	2038,46	4155319,172	333
55	2019,27	4077451,333	328
40	1982,78	3931416,528	313

From Figure 15b, the noise temperature of the amplifier is obtained by taking the negative x-intercept which is equal to 27.75 K.

$$F = 10 * \log(1 + T_n/T_o) = 10 * \log(1 + 27.75/300) = \mathbf{0.38\ dB}$$

Measurement of Carrier Temperature with amplifier noise

An example of calculating carrier temperature from the samples is presented here. In Chapter 7, Figure 27, carrier temperature for sample A is calculated. This is illustrated in Table 7. Here resistance in dark is about 85 kΩ and 2.5 kΩ under illumination.

Table 7: ***Calculation of carrier temperature***

Nr.	**Noise Voltage (a.u.)**	**Noise Power =Noise Voltage^2 (a.u.)**	$\mathbf{T_{Hot-Carriers}}$ **=300*{Noise Power / Noise Power of First Dark} * $\mathbf{R_{Sun/Dark}}$ / $\mathbf{R_{Dark}}$ (K)**
dark1	1984,15	3936851,223	300
sun1	3279,10	10752496,81	27858,67722
dark2	2278,29	5190605,324	395,539864
sun2	3676,13	13513931,78	35013,28761
dark3	2246,74	5047840,628	384,6607613
sun3	5720,11	32719658,41	84773,46411

Measurement of Carrier Temperature without amplifier noise

In Chapter 5, an optimal method is provided which attempts to eliminate the noise from the equipment. An example of calculating the carrier temperature in one of the undoped sample is presented here. The change in resistance for the undoped sample A is presented in Table 3. The corresponding noise figure to the resistance under ambient condition is noted from Figure 22. The steps described in Chapter 5 are thus performed to find the corresponding carrier temperature.

The noise of the amplifier is calculated from the noise figure corresponding to the dark resistance. For the present example, the noise figure is 0.4 dB and the resistance of the sample under dark is 85 kΩ. From eq. (5):

$$P_{Ain} = P_{in}(1 - \frac{1}{F})$$

The amplifier noise is calculated from the noise power of the first dark measurement. Thus,

$$P_{Ain} = 3936851.2231 - \frac{1}{10^{0.04}} = \mathbf{346400.2346\ a.u.}$$

The amplifier noise is subtracted from the net noise power. The carrier temperature is thus calculated from the reference using eq. (3). Thus, these carrier temperatures are plotted in Figure 27.

Table 8: ***Calculation of carrier temperature independent of amplifier noise***

Nr.	**Voltage(a.u.)**	**Noise Power =Noise Voltage^2 (a.u.)**	**Noise from Sample= Noise power recorded- Noise of Amplifier (a.u.)**	$\mathbf{T_{Hot-Carriers}}$ **=300*{Noise Power / Noise Power of First Dark} * $\mathbf{R_{Sun/Dark}}$ / $\mathbf{R_{Dark}}$ (K)**
dark1	1984,15	3936851,223	3590450,988	300
sun1	3279,10	10752496,81	10406096,58	29562,35454
dark2	2278,29	5190605,324	4844205,089	405
sun2	3676,13	13513931,78	13167531,54	37407,22884
dark3	2246,74	5047840,628	4701440,393	393
sun3	5720,11	32719658,41	32373258,18	91968,1774

APPENDIX 2

Aluminium nitride on Copper Block as a Heat Sink

To be able to measure hot carriers, it is necessary to keep the lattice cool under illumination. Thus, having an efficient heat dissipation path to keep the lattice cool, AlN is glued to a copper block as seen in Figure 7 and Figure 8. Two Copper/graphite contacts are made through electrochemical deposition and the required material is deposited or penciled (as seen for the graphite samples) between these two contacts. To be able to conclude if this setup is an efficient heat sink the following experiments are performed: As discussed earlier in Chapter 8, the penciled graphite is illuminated through the lens. Along with this, another measurement is performed where the bright spot of the sun is moved away from this graphite layer, but still on the AlN substrate. The carrier temperatures are again calculated as before along the elimination of noise. Figure 34 illustrates the carrier temperature of this experiment.

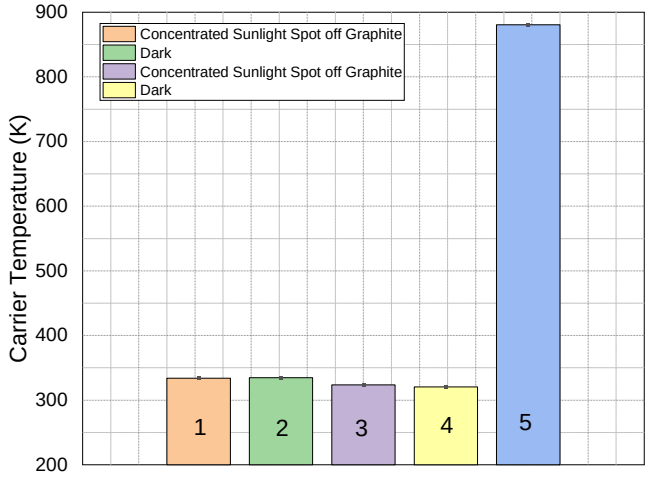

Figure 34: ***Carrier Temperature to study the heat dissipation by AlN substrate on Copper Block***

In Figure 34, "1" represents the carrier temperature when the sun's spot is away from the graphite layer while "2" represent the successive dark measurement. Similarly "3" represents the carrier temperature similar to "1" while "4" represents the dark. "5" represents the carrier temperature when the deposited layer of graphite is illuminated.

As seen in this figure, the carrier temperature when the sun's spot is off the graphite layer and the carrier temperature under dark are almost same. The sun's spot is strong enough to cause large heating of the substrate, leading to large carrier temperatures. But, when compared to "2" and "4" i.e. the dark measurements, show that the carrier temperatures are still quite near to the ambient temperature. Thus leads to the conclusion that the heat is dissipated and distributed evenly throughout the copper block and the AlN substrate and therefore, functioning like a good heat sink.